JOURNAL OF GEOPHYSICAL RESEARCH, VOL. 112, XXXXXX, doi:10.1029/2006JC003900, 2007

Upper ocean response of the Mesoamerican Barrier Reef System to Hurricane Mitch and coastal freshwater inputs: A study using Sea-viewing Wide Field-of-view Sensor (SeaWiFS) ocean color data and a nested-grid ocean circulation model

Jinyu Sheng,[1] Liang Wang,[2] Serge Andréfouët,[3] Chuanmin Hu,[2] Bruce G. Hatcher,[4] Frank E. Muller-Karger,[2] Björn Kjerfve,[5] William D. Heyman,[5] and Bo Yang[1]

Received 25 August 2006; revised 6 April 2007; accepted 25 April 2007; published XX Month 2007.

[1] The passage of category-5 Hurricane Mitch through the Mesoamerican Barrier Reef System (MBRS) in October 1998 was an extreme event with the potential to create unusual patterns of reef connectivity. The impact of this hurricane on the upper ocean of the MBRS is investigated using a triply nested grid ocean circulation modeling system. The model results are validated with contemporaneous ocean color data from the Sea-viewing Wide Field-of-view Sensor (SeaWiFS) satellite and oceanographic measurements in the MBRS. The nested grid system is forced by 6-hourly National Centers for Environmental Prediction/National Center for Atmospheric Research (NCEP/NCAR) winds for the first 294 days prior to the arrival of the hurricane in the MBRS, and then by the combination of the NCEP/NCAR wind-forcing and an idealized vortex representative of Mitch for the following 20 days. The system is also forced by the monthly mean sea surface heat and freshwater fluxes and buoyancy forcing associated with major river discharges and storm-induced precipitation in the western Caribbean Sea. The simulated upper ocean circulation during Mitch is characterized by strong and divergent currents under the storm and intense near-inertial currents and sea surface temperature cooling behind the storm. The nested grid system also reproduces the buoyant estuarine plumes extending from the coast off Honduras as inferred from SeaWiFS satellite data and detected in field measurements at Gladden Spit in Belize shortly after the passage of Hurricane Mitch. The present model results suggest that populations of site-attached organisms associated with nearshore and offshore reef features that are dynamically isolated in normal conditions experienced greater potential for ecological connection under Mitch's extreme conditions.

Citation: Sheng, J., L. Wang, S. Andréfouët, C. Hu, B. G. Hatcher, F. E. Muller-Karger, B. Kjerfve, W. D. Heyman, and B. Yang (2007), Upper ocean response of the Mesoamerican Barrier Reef System to Hurricane Mitch and coastal freshwater inputs: A study using Sea-viewing Wide Field-of-view Sensor (SeaWiFS) ocean color data and a nested-grid ocean circulation model, *J. Geophys. Res.*, *112*, XXXXXX, doi:10.1029/2006JC003900.

1. Introduction

[2] The Mesoamerican Barrier Reef System (MBRS) is the largest coral reef system in the Caribbean Sea, extending from the Bay Islands of Honduras to the northeast tip of Yucatan Peninsula of Mexico (Figure 1). Several million people live in the coastal areas of the MBRS and benefit from the natural resources provided by a network of coral structures and their biodiversity. Coral reefs in the region are affected by various natural and human disturbances and stresses including hurricanes, coral bleaching, disease outbreaks, overfishing, and contamination from land-based sources of pollution [*Kramer and Kramer*, 2002]. The MBRS is the focus of a large number of conservation and management programs.

[3] A critical factor in measures designed to preserve biodiversity and maintain the resilience and productivity of large reef tracts is the degree of connectivity that exists among individual reefs within the ecosystem [*Palumbi*,

[1]Department of Oceanography, Dalhousie University, Halifax, Nova Scotia, Canada.
[2]Institute for Marine Remote Sensing, College of Marine Science, University of South Florida, St. Petersburg, Florida, USA.
[3]UR 128 Coréus, Institut de Recherche pour le Développement, Noumea, New Caledonia.
[4]Centre for Marine Ecosystem Research, Cape Breton University, Sydney, Nova Scotia, Canada.
[5]Department of Geography and Department of Oceanography, Texas A&M University, College Station, Texas, USA.

0148-0227/07/2006JC003900$09.00

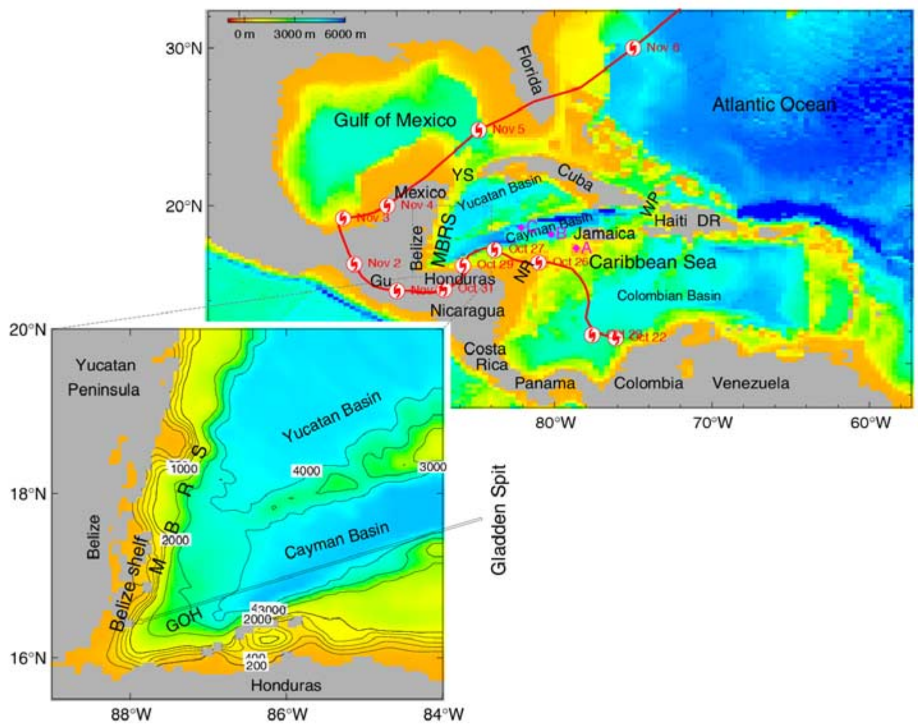

Figure 1. Topographic map of the Gulf of Mexico and Caribbean Sea (using the 2-min gridded global relief data known as ETOPO2 for this figure only. Readers are referred to Figure 5 for model topography), and the storm track (red line) of Hurricane Mitch from 22 October to 6 November 1998. The storm symbol along the storm track denotes the beginning location of the storm center on each day. Abbreviations are used for the Mesoamerican Barrier Reef System (MBRS), Yucatan Strait (YS), Gulf of Honduras (GOH), Guatemala (Gu), Nicaragua Rise (NR), Dominican Republic (DR), Windward Passage (WP), and Gladden Spit (the location of oceanographic measurements presented in Figures 3 and 4). Model results at sites A, B, and C are presented in Figures 13 and 14. The isobaths in the bottom left panel are labeled in meters.

2003]. Geographically distinct reef units act as both sources and sinks of inorganic and organic materials, of the larvae of corals, fish and other organisms that define reef community structure and function [*Hatcher*, 1997; *Sale*, 2004; *Hatcher et al.*, 2004]. Clarifying and quantifying the temporal and spatial scales of these physical and biological connections among reefs are challenges that require coupled biological-physical models of ecological connectivity under average, time-varying and extreme forcing conditions. Numerical models have been applied in this context for about twenty years, but recent demand for ecosystem-based management practices based on scientific knowledge has accelerated development of these models [*Wolanski*, 2001; *Cowen et al.*, 2006; *Tang et al.*, 2006].

[4] Quantification of hydrodynamic connections of dense matrices of reefs within a large ocean management area requires reliable ocean circulation models with spatial resolutions adequate to resolve individual reef structures and the upper layer of the water column where bioparticles reside. There are several model options. Finite difference models with a very high resolution grid throughout the entire domain are ideal, but processing times are prohibitive. Finite element models with variable mesh size grid are popular, but designing grids useful for Lagrangian tracking is problematic [*Legrand et al.*, 2006]. A third option is to embed finer-resolution finite difference submodels within a coarser regional model [*Oey and Chen*, 1992; *Sheng et al.*, 2005]. Patterns of physical connectivity in a given area evolve on timescales spanning hours to years, depending on a variety of factors such as the tidal regime, wind-forcing or global climate change. Climatological oceanographic data can be used to derive average connectivity patterns on timescales approximating the life cycles of reef organisms, but extreme and sporadic events such as hurricanes and tropical storms will generate unusual, short-term patterns. Successful simulations of these patterns could reveal important transfers among reef populations, especially if they are concurrent with fish or coral spawning periods. Parameterizing, calibrating and validating extreme-event models poses yet another level of challenge, which must be addressed with synoptic observation tools.

[5] The main objectives of this study are to study the effect of a major hurricane event on the upper ocean circulation of the MBRS using a nested-grid modeling system, and to use the satellite imagery and field data collected during the event to evaluate the numerical results. In October 1998, the Sea-viewing Wide Field-of-view Sensor (SeaWiFS) captured dispersal patterns of fresh water plumes that traced connections between land and various reefs immediately following landfall of Hurricane Mitch in Honduras [*Andréfouët et al.*, 2002]. River plumes originating along the northern Honduras coast reached reefs in

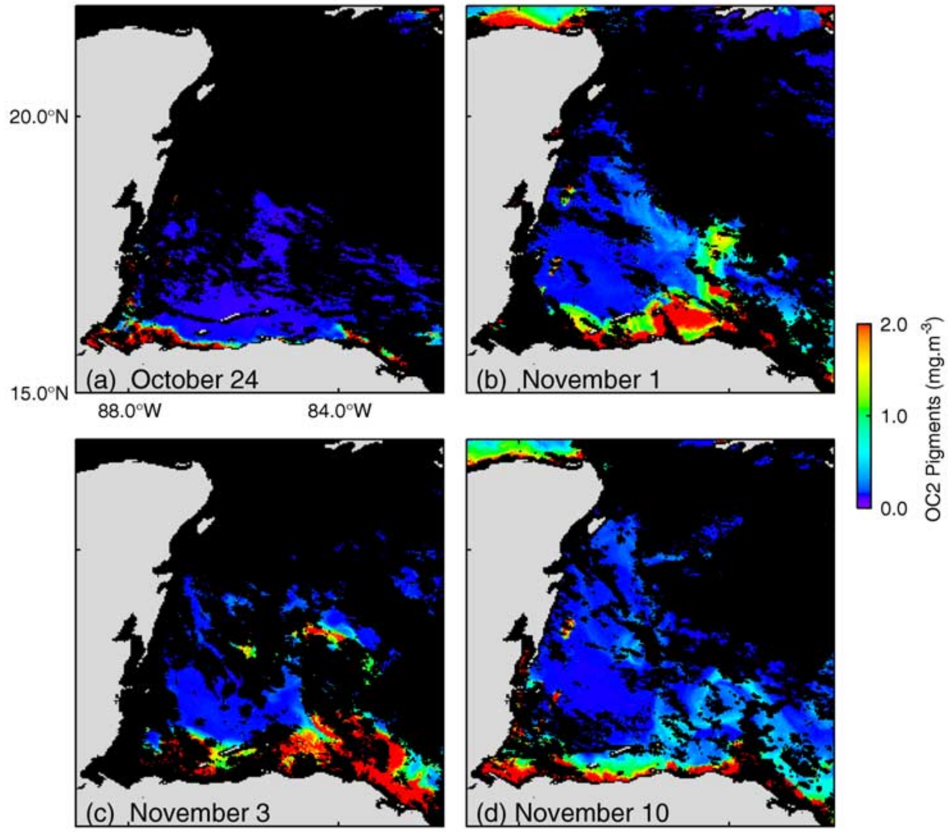

Figure 2. Spatial patterns of turbid coastal water plumes on the MBRS derived from SeaWiFS remote sensing data during and after Hurricane Mitch in Autumn 1998 [*Andréfouët et al.*, 2002]. The images were obtained using the SeaWiFS Data Analysis System (SeaDAS V4.4) distributed by NASA, where chlorophyll-a pigment concentrations were estimated using the OC2 algorithm of *O'Reilly et al.* [1998]. Clouds and land are masked as black and grey colors, respectively. (a) Typical dry season conditions showing clear ocean and narrow zones of turbidity near the river mouths. (b) First cloud-free image 3 days after landfall of Mitch showing a large-scale plume that covered most of the Bay Islands and extended to 200 km from its origin. (c) The coastal water plume extended farther northward to reach Glovers atoll on the Belize shelf. (d) The plume dissipated by dilution.

Belize and Mexico (Figure 2). Numerical models have already been developed to study connectivity in the MBRS under climatological (monthly mean) conditions [*Tang et al.*, 2006] and eddies influence [*Ezer et al.*, 2005]. Here we ask whether extreme forcing of the simple and effective parameterizations of one of these models can reproduce surface ocean circulation events at temporal and spatial scales relevant to ecological connectivity. Hurricane Mitch provides an ideal case study. In this study we use the modified version of the nested-grid model system developed by *Tang et al.* [2006] with reasonable representation of model forcing associated with the storm, and demonstrate how remotely sensed data can be used to evaluate the pattern of physical connectivity associated with the extreme event.

[6] The structure of this paper is as follows. Section 2 summarizes the general mean circulation within the MBRS and provides a brief review of numerical modeling of hurricane-induced circulation. Section 3 presents the remotely sensed and in situ observations collected during Mitch, and describes the triply nested-grid modeling system and external forcing. Section 4 discusses the model results, including near-surface and subsurface currents, SST cooling, patterns of river plume dispersal and reef connectivity. Section 5 provides a brief summary and discussion.

2. Background

2.1. Observed and Simulated Ocean Circulation in the MBRS Under Normal Conditions

[7] Many different types of three-dimensional ocean circulation models have been used to study the large-scale circulation of the Caribbean Sea [*Murphy et al.*, 1999; *Ezer et al.*, 2003; *Sheng and Tang*, 2003; *Ezer et al.*, 2005; *Oey et al.*, 2005; *Tang et al.*, 2006; *Oey et al.*, 2006, 2007]. The recent studies by *Sheng and Tang* [2003, 2004], *Ezer et al.* [2005], and *Tang et al.* [2006] focus specifically on the western Caribbean Sea (WCS) and the MBRS. *Sheng and Tang* [2004] used a doubly nested-grid system to study the monthly mean circulation in the MBRS that featured a finer-resolution (~6 km) inner model embedded in a coarse-resolution (~20 km) model for the WCS. *Tang et al.* [2006] used a triply nested-grid system with horizontal resolutions

of ~20 km, 6 km and 2 km to study the upper ocean circulation and hydrodynamic connectivity associated with the reef atolls on the Belize shelf. By using the Princeton Ocean Model with a variable horizontal resolution ranging from 3 km along the MBRS to 8 km on the open boundary, *Ezer et al.* [2005] examined the influence of topography, circulation, wind, density and eddies on 3D circulation in the MBRS. All of these models reproduce the general circulation patterns inferred from sparse and rare empirical observations. Little is known, however, about the detailed, interreef circulation within the MBRS during sporadic or extreme events.

[8] Historical observations compiled by *Craig* [1966] identify three distinct features of the general mean circulation in the upper ocean of the MBRS region [see also *Ezer et al.*, 2005]: an intense northwestward offshore flow as part of the Caribbean Current in the deep water off the continental shelves of Honduras and Belize; an equatorward coastal current that flows first along the east coast of Belize and then eastward along the northern coasts of Guatemala and Honduras; and a cyclonic (counterclockwise) circulation in the Gulf of Honduras (GOH) [*Heyman and Kjerfve*, 2000]. As discussed by *Ezer et al.* [2005], two subsurface drifters were deployed in April 2000 at 15 m, one to the south and one to the west of Glover's Reef. The first drifted southward and then eastward, following a cyclonic gyre in the GOH. The second drifted northward about 200 km in 20 days, indicating a northward flow from Glover's Reef and through the passage between Turneffe Islands and Lighthouse Reef Atolls. Unlike the first trajectory, this northward current was in the direction opposite to the general mean circulation pattern suggested by *Craig* [1966]. *Ezer et al.* [2005] attributed this discrepancy to the mesoscale variability of the near-surface circulation in the region.

2.2. Numerical Studies of Hurricane-Induced Circulations

[9] Various numerical studies have examined storm-induced circulations in coastal and open ocean waters [*Chang and Anthes*, 1978; *Price*, 1981; *Greatbatch*, 1983; *Sheng et al.*, 2006; *Oey et al.*, 2006, 2007]. *Price* [1981] suggested a simple parameterization for estimating the vertical eddy viscosity and diffusivity coefficients in the upper ocean in terms of the mean velocity difference across the base of the mixed layer. With Price's parameterization, *Sheng et al.* [2006] simulated the storm-induced currents on the Scotian Shelf and adjacent deep waters associated with Hurricane Juan in 2003. *Oey et al.* [2006, 2007] studied the response of the Caribbean Sea and Gulf of Mexico to Hurricane Wilma in 2005 using the Princeton Regional Ocean Forecast System. Together, these studies demonstrate that the upper ocean response to a moving storm can be characterized as intense inertial oscillations and sea surface cooling in the storm wake, biased to the right of the storm track, and strongly dependent on the hurricane translation speed. Intensive vertical mixing induced by the pressure-driven displacement of the sea surface elevation and the wind-driven vorticity results in significant drops in sea surface temperature (SST), typically from 1 to 6°C, behind a moving storm [*Jordan*, 1964; *Fedorov et al.*, 1979; *Smith*, 1982; *Cornillon et al.*, 1987]. These models, however, do not deal well with the evolution of the density field associated with storm-induced inputs of fresh water, which are important in reef-bound coastal seas such as the MBRS. Our study places special emphasis on storm-induced currents and density variations in the upper layer of the MBRS during Hurricane Mitch because these attributes may strongly influence patterns of ecological connectivity.

3. Methods: Observations During Mitch and Nested-grid Modeling System

3.1. Remotely Sensed and in Situ Observations During Hurricane Mitch

[10] Hurricane Mitch devastated areas in the Central American countries of Nicaragua, Honduras, El Salvador and Guatemala, resulting in more than 9,000 human deaths. The storm originated from a tropical wave over western Africa on 8 October 1998 and moved through the eastern Caribbean Sea on 18 and 19 October (http://www.nhc.noaa.gov). Mitch intensified from a tropical depression to a hurricane in the southwestern Caribbean Sea on 22 October (Figure 1), with a maximum wind speed of ~55 km h^{-1}. By 26 October, the storm had strengthened to a Saffir-Simpson category-5 hurricane, with a maximum sustained wind speed of ~285 km h^{-1}. From 27 October, Mitch traveled east, parallel to and some 60 km off the Honduras coast, turned sharply south, then became nearly stationary over Guanaja in the Bay Islands for over 24 hours, eventually drifting slowly south. The storm made landfall over Honduras during the morning of 29 October with a maximum wind speed of ~160 km h^{-1}. Mitch progressed inland to the south then westward over the mountainous regions of Honduras and Guatemala. During its passage, Mitch generated between 0.17 m and 1.9 m of precipitation over much of Nicaragua, Honduras, and Guatemala, which in turn caused intense flooding and land slides [*Guiney and Lawrence*, 1999], and massive river discharge to the adjacent coast [*Smith et al.*, 2002].

[11] Synoptic satellite imagery provides critical information for the calibration and verification of numerical models of atmospheric and oceanic circulations [*Ishizaka*, 1990]. Remotely sensed data can map the time-evolving distribution of low-salinity waters near the coast [*Andréfouët et al.*, 2002; *Hu et al.*, 2004, 2005]. SeaWiFS images collected after Hurricane Mitch provide a clear picture of coastal runoff because the river plumes have a color different from the more transparent waters of the western Caribbean Sea. This capability can be used to measure the displacement of density fronts associated with differences in water salinity [*Hu et al.*, 2004]. SeaWiFS images have been used to demonstrate an advective connection between nearshore and offshore areas of the MBRS [*Andréfouët et al.*, 2002]. On 24 October, prior to the arrival of Hurricane Mitch, turbid water was restricted to the Honduras coast and Belize shelf (Figure 2a). After Mitch, the turbid plume extended from the northeast coast of Honduras to the deep ocean, the Bay Islands (150 km, eastward, Figure 2b), and further north to the Belize shelf on November 3 (Figure 2c).

[12] SeaWiFS high-resolution (1.1 km/pixel at nadir) data were captured and processed at the University of South Florida using the software package SeaDAS4.4. After several rounds of reprocessing to incorporate calibration and algorithm updates, the data products (such as distributions of

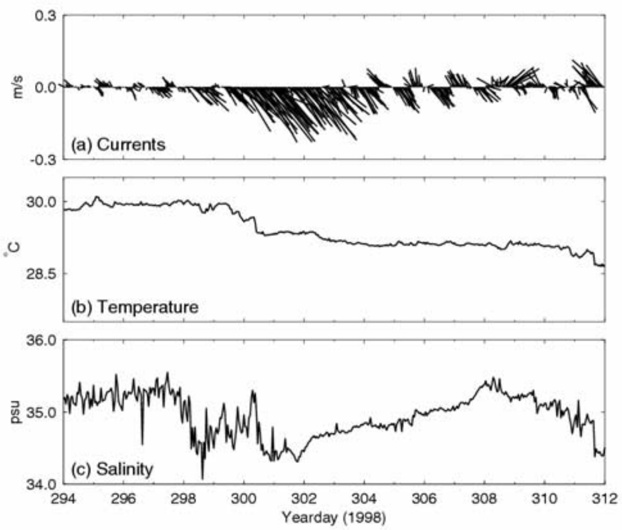

Figure 3. Observed (a) currents, (b) temperature, and (c) salinity made by a current meter deployed at 5 m above the bottom in a water depth of 27 m at and 87.95°W 16.5°N off Gladden Spit at the southern end of the Belize Barrier Reef (see Figure 1) over an 18-day time series (22 October to 8 November 1998) spanning the passage of Hurricane Mitch through the area.

chlorophyll-a concentration) are considered to be of high scientific quality [*McClain et al.*, 2004]. We used the SeaWiFS ocean color data to evaluate the numerical model results of our study by inferring the distribution of low-salinity surface waters derived from terrestrial discharge associated with the hurricane. First we derived the back-scattering coefficient (b_{bp}) and the total combined absorption coefficient due to colored dissolved organic matter (CDOM) plus detritus (i.e., $a_{CDM} = a_{CDOM} + a_D$, [m^{-1}]) using remote sensing reflectance in the visible bands (412, 443, 490, 510, 555, and 670 nm, respectively) in a semianalytical algorithm [*Lee et al.*, 2002]. An empirical equation was then used to estimate a_D ($a_D(440) = 2.075 \times (b_{bp}(555))^{1.02}$; $n = 110$, $r = 0.89$, $0.001 < a_D(440) < 0.12$). This relationship was derived from field data collected on eight oceanographic cruises on the western Florida Shelf in 2000 and 2001 (J. Cannizzaro, University of South Florida, unpublished data, 2006). We calculated $a_{CDOM}(440)$ from $a_{CDM}(440)$ by subtracting $a_D(440)$. The $a_{CDOM}(440)$ values were converted to salinity using the relationship Salinity = $36.1 - 10a_{CDOM}(440)$ ($0 < a_{CDOM}(440) < 3.61$ m^{-1}). This empirical approach is still experimental, but is based on extensive research on the inverse relationship between a_{CDOM} and sea surface salinity [e.g., *Ferrari and Dowell*, 1998; *D'Sa et al.*, 2002; *Hu et al.*, 2003, 2004]. Unfortunately, no in situ measurements of surface salinity were available to calibrate this relationship in the MBRS during the study period. The purpose, however, is to determine if the model can reproduce the spatial pattern of low-salinity water (river plumes), rather than the absolute salinity of those features.

[13] An InterOcean S4 electromagnetic current meter was moored at 1 km seaward (east) of the MBRS at Gladden Spit (87.95°W, 16.50°N) of Belize during the passage of Hurricane Mitch. The instrument was moored 5 m off the bottom (i.e., at 27 m depth), less than 10 m from the edge of a submarine cliff where the seabed plunges to more than 600 m. The instrument recorded currents, temperature, and salinity for 18 days starting on 22 October 1998 (day 294; Figure 3). Every hour on the hour, the S4 recorded an average of 240 measurements at 2 Hz frequency during a 2 min period. CTD casts were made with a Seabird SBE9 to 70 m depth in deep water adjacent to the current meter, on 5 December 1998, five weeks after the passage of Hurricane Mitch, and again in May 1999, five months later (Figure 4). These data collected at a seamark on the boundary between the deep ocean in the outer Gulf of Honduras and the

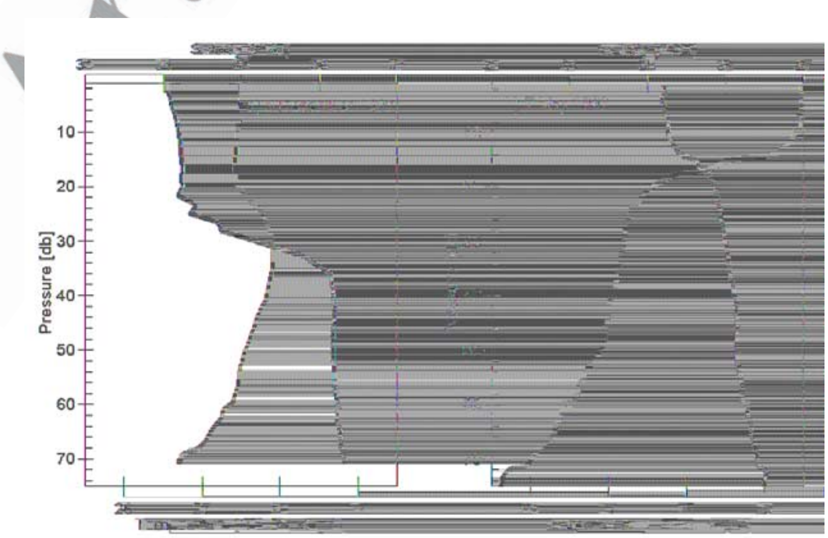

Figure 4. CTD measured salinity and temperature as a function of pressure to ~70 m depth, 2 km east of Gladden Spit at 16.5°W and 87.933°N and (see Figure 1) on: (a) 5 December 1998, 5 weeks after the passage of Hurricane Mitch where surface salinity was reduced to 34.0 psu at 23 m depth, and (b) 7 May 1999, 6 months after the storm when surface salinity had returned to normal values of 35.5 psu.

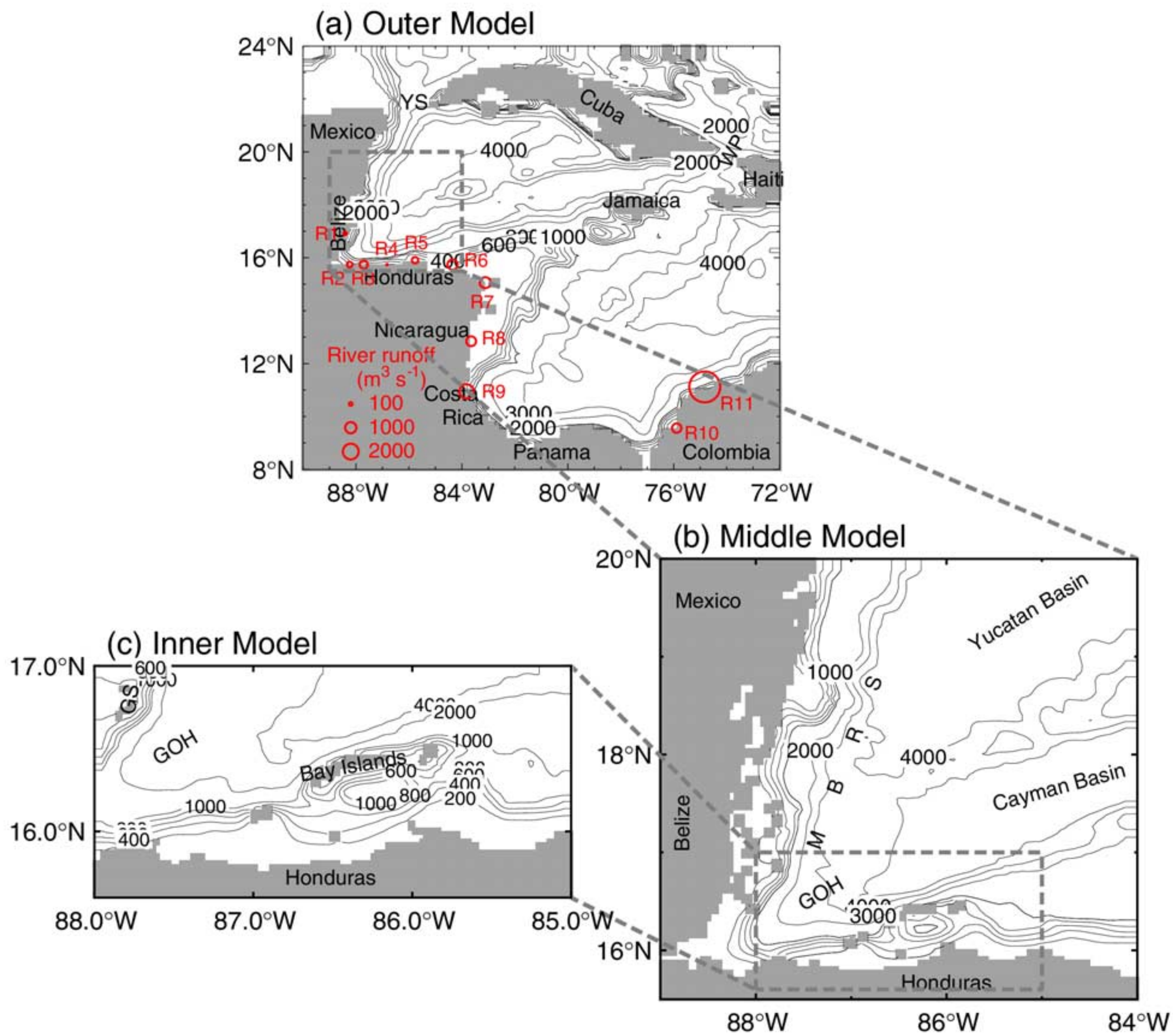

Figure 5. Selected coastal and bottom topographic features for the triply nested-grid modeling system consisting of (a) an outer model covering western Caribbean Sea (WCS), (b) a middle model including the southern Mesoamerican Barrier Reef System (MBRS), and (c) an inner model focused on the north coast of Honduras and Bay Islands. Abbreviations are used for the Mesoamerican Barrier Reef System (MBRS), Yucatan Strait (YS), and Gulf of Honduras (GOH). Isobaths are labeled in units of meters, and open red circles denote the positions of the mouths of 11 major rivers specified in the modeling system. The strength of the annual mean discharge of each river is denoted by the size of each circle.

southernmost extent of the contiguous barrier reef, span the passage of the hurricane and provide the sole Eulerian validation of the model predictions.

3.2. Triply Nested-grid Ocean Circulation Modeling System

[14] The numerical model used in this study is the modified version of the triply nested-grid ocean circulation modeling system developed by *Tang et al.* [2006], which was constructed from a primitive-equation z-level model known as CANDIE (the Canadian version of Diecast) [*Sheng et al.*, 1998]. CANDIE has been successfully applied to address various modeling problems in continental shelf seas, including wind-driven circulation over an idealized coastal canyon [*Sheng et al.*, 1998], a density-driven coastal current [*Sheng*, 2001], and seasonal circulation in the northwestern Atlantic Ocean [*Sheng et al.*, 2001]. Most recently CANDIE has been applied to the WCS [*Sheng and Tang*, 2003, 2004; *Tang et al.*, 2006], Lunenburg Bay in Nova Scotia [*Sheng and Wang*, 2004; *Wang et al.*, 2007], and Lake Huron and Georgian Bay [*Sheng and Rao*, 2006].

[15] The nested-grid system has three subcomponents (Figure 5): a coarse-resolution (~19 km) outer model covering the WCS (72°W–90°W, 8°N–24°N), an intermediate-resolution (~6 km) middle model covering the MBRS (84°W–89°W, 15.5°N–20°N), and a fine-resolution (~2 km) inner model covering the northern coast of Honduras and the Bay Islands (85°W–88°W, 15.6°N–17°N).

Table 1. Center Depths and Thicknesses of 28 Z-Levels Used in the Triply Nested, Finite Difference Circulation Modeling System of the MBRS

Z-Level	Depth, m	Thickness, m
1	1	2
2	3	2
3	5	2
4	7	2
5	9	2
6	11	2
7	13	2
8	15	2
9	17	2
10	19	2
11	25	10
12	40	20
13	75	50
14	140	80
15	230	100
16	340	110
17	450	110
18	575	150
19	725	150
20	900	200
21	1250	500
22	1750	500
23	2250	500
24	2750	500
25	3250	500
26	3750	500
27	4250	500
28	4750	500

The time steps are set to 14.4, 5.5, and 2.2 min in the three submodels respectively. The nested system uses the digital bathymetric database of 2-min resolution (DBDB2) developed by the Ocean Dynamics and Prediction Branch, U.S. Naval Research Laboratory. The boundary definitions of the middle and inner model domains are selected to focus on the dispersal patterns of the coastal runoff plumes detected by the SeaWiFS along the Honduran coast.

[16] The three subcomponents of the nested system have the same 28 unevenly spaced z-levels, with a finest vertical resolution of 2 m in the top ten levels, and relatively coarse vertical resolution of about 500 m at depths of greater than 1000 m (Table 1). The nested-grid system is very similar to the one used by *Tang et al.* [2006], except that (1) the inner model domain in this study covers the coastal region of Honduras, the Bay Islands, and Gulf of Honduras; (2) the vertical resolution of the nested-grid system is finer in the top 20 m; (3) model external forcing includes a simple vortex to represent Mitch wind-forcing and buoyancy forcing associated with river discharges and storm-induced precipitations in the WCS; and (4) the vertical mixing scheme suggested by *Price* [1981] is used.

[17] The nested-grid system uses the subgrid-scale vertical mixing parameterization suggested by *Price* [1981] for the vertical eddy viscosity and diffusivity coefficients K_m and K_h. In this scheme, a scaled velocity (ΔV), defined as the magnitude of the mean velocity difference across the base of the upper ocean mixed layer, is used to parameterize the vertical mixing coefficients. This led to realistic storm simulations showing a stronger sea surface temperature response to the right of the storm track [*Sheng et al.*, 2006]. The horizontal mixing scheme of *Smagorinsky* [1963] with a coefficient of 0.1 is used to parameterize the horizontal eddy viscosity and diffusivity coefficients (A_m, A_h), which are related to the model grid spacing (Δx, Δy), and velocity shear and strain in the horizontal direction. Since the scheme discussed by *Smagorinsky* [1963] is resolution-dependent, the parameterization of horizontal mixing is different in each submodel of the nested system. The nested system also uses the fourth-order numerical technique [*Dietrich*, 1997] and flux limiter to discretize the nonlinear advection terms [*Thuburn*, 1996].

[18] The two-way nesting technique based on the smoothed semiprognostic method developed by *Sheng et al.* [2005] is used to exchange information between three subcomponents of the nested-grid system. A free-slip boundary condition is used at lateral solid boundaries in the three subcomponents of the system. Along the open boundaries of each subcomponent, the normal flow, temperature and salinity fields are updated using adaptive open boundary conditions [*Marchesiello et al.*, 2001]. The depth-mean normal flows across the outer model open boundaries are set to be the monthly mean results produced by a (1/3)° Atlantic model based on FLAME. The outer (middle) model results are used to specify the boundary conditions along the open boundaries of the middle (inner) models.

3.3. Initial Condition and External Forcing

[19] The nested-grid circulation system is initialized with the monthly mean climatology of temperature and salinity in January constructed from hydrographic observations at the standard z-levels extracted from the World Ocean Database 1998 compiled by the U.S. National Oceanic and Atmospheric Administration's National Oceanographic Data Center (NOAA-NODC), using the objective analysis technique known as Barnes' algorithm [*Geshelin et al.*, 1999].

[20] In the first 294 days (i.e., from 1 January to 21 October 1998) of model integrations prior to the arrival of Mitch in the MBRS, the nested-grid system is forced by 6-hourly wind stress, monthly mean heat and freshwater fluxes at the sea surface, and climatologically time-mean freshwater discharges from 11 major rivers in the WCS. The wind stress is derived from 6-hourly wind velocity extracted from the National Centers for Environmental Prediction (NCEP) and the National Center for Atmospheric Research (NCAR) 40 year reanalysis (known as NCEP/NCAR data set [*Kalnay et al.*, 1996]). The conventional bulk formula of *Large and Pond* [1981] is used to convert NCEP/NCAR wind velocities to wind stresses, except that the drag coefficient is set to a constant of 2.2×10^{-3} if the NCEP/NCAR wind speed is greater than 33 m s^{-1} [*Powell et al.*, 2003].

[21] The net heat flux through the sea surface Q_{net} is expressed according to *Barnier et al.* [1995]:

$$Q_{net} = Q^c_{net} + \gamma(SST^c + SST^m) \tag{1}$$

where Q^c_{net} is the monthly mean net heat flux [*da Silva et al.*, 1994], SST^c is the monthly mean sea surface temperature climatology, SST^m is the model calculated sea surface temperature, and γ is the coupling coefficient defined as $\Delta z_1 \rho_o c_p / \tau_Q$, where Δz_1 is the thickness of the top z-level, c_p is the specific heat, and τ_Q is the restoring timescale which is set to 10 days. The model sea surface salinity is also restored to the monthly mean climatology with the same restoring timescale.

Table 2. Estimated Drainage Areas and Average Discharge of 11 Major Rivers in the Western Caribbean Sea, and Estimated Peak Discharge of Five Major Rivers in Honduras and Guatemala During Mitch in 1998[a]

River/Country	Drainage Area, km^2	Average Discharge, m^3 s^{-1}	Peak Discharge During Mitch, m^3 s^{-1}
Sarstún and Dulce/Belize-Guatemala	6352(4)–10,604(6)	96(5)–333(6)	-
Motagua/Guatemala	16,544(6)	165(6)–186(7)	24,219(5)
Ulua/Honduras	25,710(6)	334(6)–526(1)	32,838(3)
Cangrejal-Bonito/Honduras	564(3)–717(6)	7(6)–16(5)	10,390(3)
Aguan/Honduras	10,580(2)–10,684(6)	108(6)–300(5)	27,939(3)
Patuca/Honduras	23,064(6)–25,600(1)	239(6)–825(1)	28,672(3)
Coco/Honduras-Nicaragua	26,700(1)	950(1)	-
Grande de Matagalpa/Nicaragua	19,700(1)	762(1)	-
San Juan/Nicaragua-Costa Rica	38,900(1)	1,620(1)	-
Sinu/Colombia	4200(1)	700(1)	-
Magdalena/Colombia	235,000(1)	7500(1)	-

[a]Data sources for the estimations are given in parentheses: (1) *United Nations Environment Programme Chemicals* [2002]; (2) *Mastin and Olsen* [2002]; (3) *Smith et al.* [2002]; (4) taken from: http://www.biodiversity.bz/find/watershed/profile.phtml?watershed_id=3 (only the drainage area within Belize considered); (5) estimated using the observations of the nearby rivers; (6) *Burke and Zugg* [2006]; (7) *Thattai et al.* [2003].

[22] Eleven major rivers are specified in the top z-level of the nested-grid system (see Figure 5 for positions of river mouths). Each river is approximated to be one grid cell wide at the river mouth and 3, 5 and 10 grid cells long (i.e., upstream) in the outer, middle model, and inner submodels, respectively. The climatological time-mean discharge of each river derived from estimates made by *Mastin and Olsen* [2002], *United Nations Environment Programme Chemicals* [2002], *Thattai et al.* [2003], and *Burke and Zugg* [2006] (Table 2) is applied for the first 294 days of the model run to 21 October 1998 (prior to the hurricane). Among these rivers, the Magdalena River in Colombia has the largest time-mean discharge ($\sim$7.5 $\times$ 10^3 m^3 s^{-1}) and the combination of the Cangrejal and Bonito Rivers in Honduras has the smallest ($\sim$16 m^3 s^{-1}). The discharge of each river is specified in the term for vertical velocity at the bottom of the grid cell located at the head (i.e., most inland grid cell) of the river. On the basis of the salt conservation, the model salinity (S_r^n) at the river head in the model is specified as

$$S_r^n = \frac{S_r^{n-1} \cdot V_c + S_0 \cdot V_r}{V_c + V_r}, \qquad (2)$$

where S_r^{n-1} is the model salinity at the head in the previous time step; S_0 is the salinity at the head, which is set to 0.4 psu; V_c is the volume of the model cell at the head; and V_r is the volume of freshwater discharge from the river during one time step. This specification allows the buoyant, estuarine waters to flow freely into the WCS with the model salinity at the river mouth varying according to the strength of the river discharge.

[23] During the next 20 days of model simulations from 22 October to 10 November, the nested-grid system is forced by three additional terms associated with the storm. The first is a simple vortex to represent storm wind stress associated with Mitch (C. Fogarty, personal communication, 2007),

$$\tau(r) = \begin{cases} \tau_{\max} \dfrac{r}{r_{\min}} & r < r_{\min} \\ \tau_{\max} \dfrac{r_{\max} r_{\min}}{r_{\max} r_{\min}} \left(\dfrac{1}{r} - \dfrac{1}{r_{\max}} \right) & r_{\min} \le r \le r_{\max} \\ 0 & r > r_{\max} \end{cases}, \qquad (3)$$

where $\tau(r)$ is the cyclonic wind stress as a function of radius r with respect to the center of the moving storm, $\tau_{\max}$ is the amplitude of the maximum wind stress located at $r_{\min}$, and $r_{\max}$ is the outer radius where τ vanishes. Here $r_{\min}$ is set to 20 km and $r_{\max}$ to 300 km based on the satellite images collected during Hurricane Mitch. Here $\tau_{\max}$ is the maximum wind stress calculated from the observed maximum sustained wind speed provided by the U.S. Southeast Regional Climate Center (SERCC). The realistic storm track provided by SERCC (Figure 1) is also used in the study, with the instantaneous translational speeds of Hurricane Mitch calculated from the 6-hourly SERCC storm track data.

[24] Figure 6 shows the combination of the NCEP/NCAR wind stress and the parameterized vortex at four different times during Mitch. On day 295.5 (1200 UTC 23 October), the vortex is located over the southwestern Colombian Basin, with a maximum wind stress of $\sim$1 N m^{-2} (Figure 6a). On day 298.5 (1200 Universal Time Coordinated (UTC) 26 October) the vortex reaches the northern flank of the Nicaragua Rise (Figure 6b), with a maximum stress of about 10 N m^{-2}. The vortex approaches the northern coast of Honduras and made landfall during the early morning of 29 October, with a maximum wind stress of $\sim$2.5 N m^{-2} (Figure 6c). On day 304.5 (1200 UTC 1 November), the combined wind stress is relatively uniform and roughly westward at $\sim$0.1 N m^{-2} in the WCS except for the southern MBRS and southwestern Columbian Basin. The combined wind stress in the southern MBRS is roughly northwestward on day 301 (Figure 6d).

[25] The second additional term is the buoyancy forcing associated with Mitch-induced precipitation on the ocean surface. Figure 7 shows the daily mean precipitation in the WCS during Mitch interpolated from the 1° $\times$ 1° global precipitation data set constructed by *Huffman et al.* [2001] from multisatellite observations. On day 295.5, the storm-induced rainfall was heavy over the southeastern Colombian Basin and light over other regions of the WCS. On day 298.5 heavy rainfall occurred over the northern Caribbean Sea with a maximum of $\sim$90 mm d^{-1} (Figure 7b). The daily mean precipitation was about 20 to 30 mm d^{-1} over the southern MBRS just before Mitch made landfall (Figure 7c). Since evaporation was relatively

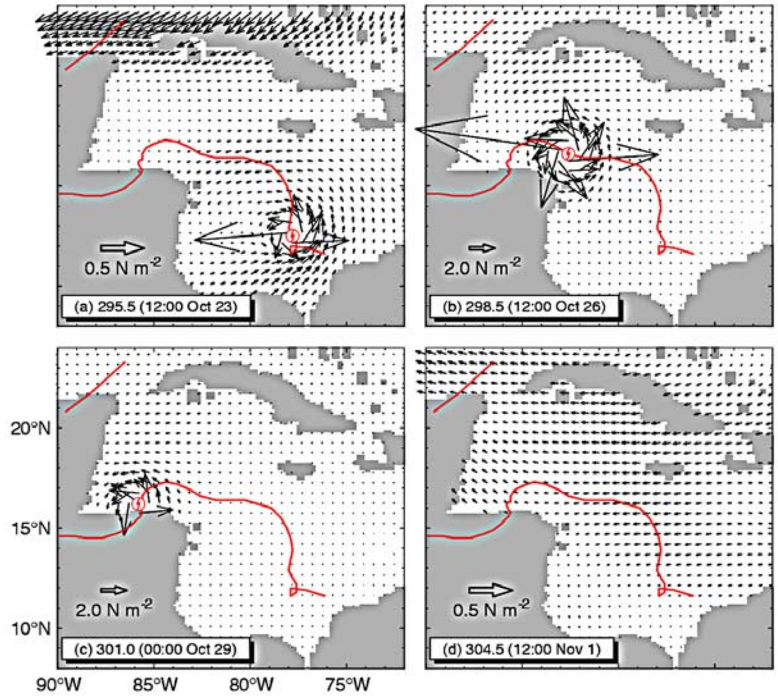

Figure 6. Combined wind stress based on 6-hourly NCEP/NCAR fields and a simple vortex at (a) day 295.5 (1200 UTC 23 October), (b) day 298.5 (1200 UTC 26 October), (c) day 301.0 (0000 UTC 29 October), and (d) day 304.5 (1200 UTC 1 November) during Hurricane Mitch in 1998. Wind stress vectors are plotted at every third model grid of the outer model.

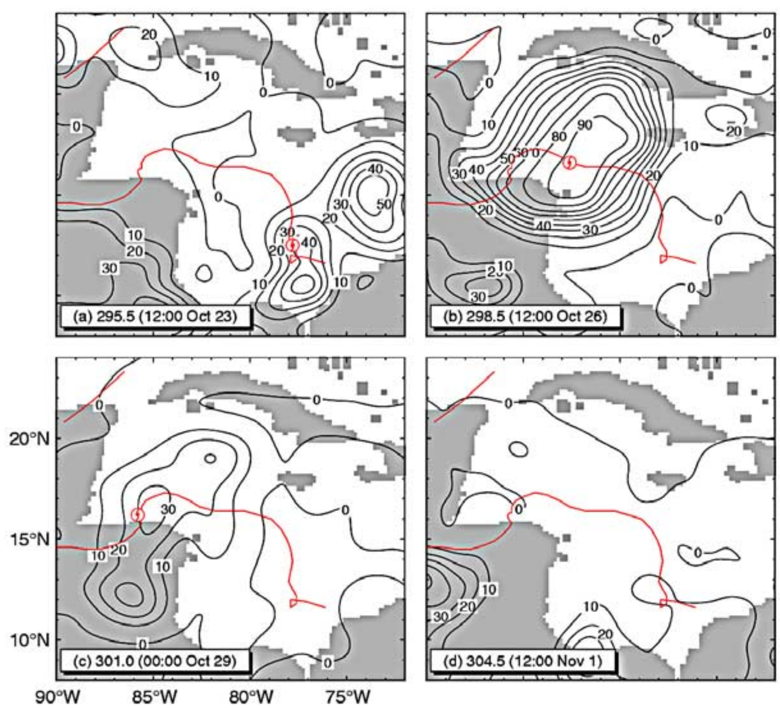

Figure 7. Daily mean precipitation during Hurricane Mitch, extracted from the data set produced by *Huffman et al.* [2001] at: (a) day 295.5 (1200 UTC 23 October), (b) day 298.5 (1200 UTC 26 October), (c) day 301.0 (0000 UTC 29 October), and (d) day 304.5 (1200 UTC 1 November) of 1998. Contour interval is 10 mm/day.

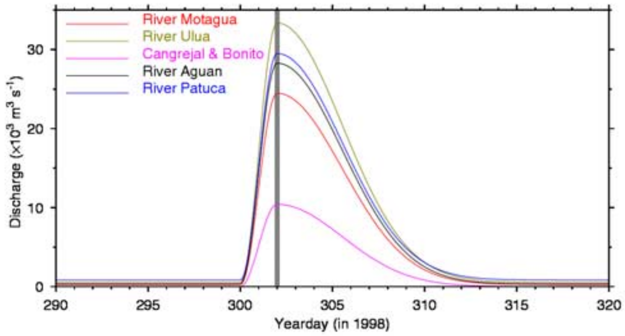

Figure 8. Modeled time series of freshwater discharge from 5 major rivers in Honduras (see Figure 5) to the southern Mesoamerican Barrier Reef System during Hurricane Mitch.

small in comparison with heavy precipitation in the WCS during Mitch, the model salinity in the top z-level affected by storm precipitation (S_1^n) can be estimated by

$$S_1^n = \frac{\hat{S}_1^n \cdot \Delta z_1 + S_{00} \cdot \Delta z_p}{\Delta z_1 + \Delta z_p}, \tag{4}$$

where $\hat{S}_1^n$ is the model salinity in the top z-level before the modification; S_{00} is the salinity of rainwaters, which is set to 0; Δz_1 is the thickness of the top z-level; and Δz_p is the thickness of the rainfall during one time step.

[26] The third additional term is buoyancy forcing associated with storm-induced discharge from 5 major rivers in Honduras and Guatemala (i.e., the Motagua, Ulua, Cangreja, Bonito, and Aguan Rivers; see Table 2 and Figure 5) during Mitch. The peak discharge (estimated from indirect measurements [see *Smith et al.*, 2002]) from the five major rivers during Mitch was $\sim$1.3 $\times$ 10^5 m^3 s^{-1}; about 70 times larger than the climatological mean discharge of $\sim$1.9 $\times$ 10^3 m^3 s^{-1} (Table 2). Since there were no direct river gauge measurements, time series of the storm-induced runoff from these five rivers are constructed (Figure 8) by assuming the Mitch-induced floods started on day 300.0, reached the peak discharge on day 302.0 and then decreased exponentially with an e-folding time of 5 days.

3.4. Numerical Experiments

[27] Five numerical experiments (Table 3) are conducted to examine the sensitivity of the nested-grid system to the buoyancy forcing associated with river runoff along the coastal boundary and storm-induced precipitation over the open water of the WCS. These experiments are run for the 20-day period from 22 October to 10 November as follows.

[28] 1. In the control run (Exp-Control) the nested-grid system is forced by the combined wind stress (i.e., the combination of the 6-hourly NCEP/NCAR wind stress and the parameterized vortex), monthly mean sea-surface heat and freshwater fluxes, storm-induced precipitation in the open ocean of the WCS, and combined freshwater discharge from 11 major rivers (i.e., the combination of Mitch-induced runoff from 5 major rivers in Honduras and Guatemala and time-mean runoff from 6 other major rivers in the WCS).

[29] 2. In the normal run (Exp-Norm) the system is forced by monthly mean sea-surface heat and freshwater fluxes, 6-hourly NCEP/NCAR wind-forcing and time-mean discharge from 11 rivers in the WCS but without the parameterized vortex associated with Mitch and without buoyancy forcing associated with storm-induced precipitation and storm-induced river runoff. Since the horizontal resolution of the NCEP/NCAR reanalysis data is $\sim$200 km in the WCS, which is too coarse to resolve Hurricane Mitch, the model results in Exp-Norm are used to represent the ocean circulation without the storm effect.

[30] 3. In the extreme run (Exp-bigRunoff) the model forcing in this run is the same as in the control run except for much stronger (maximum estimates, Table 2) freshwater discharge from the 5 major rivers in Honduras and Guatemala. The same river flooding start time and peak values before day 302 are used in this run, but they decrease more slowly with an e-folding time of 10 days rather than 5 days used in the control run.

[31] 4. In the average run (Exp-AvgRunoff) the model forcing is the same as in the control run except that the time-mean river discharge estimated during Mitch is applied for the 20-day period.

[32] 5. In the dry run (Exp-noRain) the model forcing is the same as in the control run except for the exclusion of the storm-induced precipitation (Table 3).

[33] All other model parameters are the same in the five experiments. The model results presented in section 4 are those produced by the system in the control run except where otherwise noted.

4. Model-Calculated Upper Ocean Response to Hurricane Mitch

4.1. Simulated Ocean Currents

[34] At day 295.5 (1200 UTC October 23) the parameterized vortex is located in the southern Colombian Basin, and the simulated (control run) near-surface circulation in a radius of approximately 100 km around the storm center is characterized by divergent currents of $\sim$1 m s^{-1} (Figure 9). Outside this area of influence the near-surface circulations

Table 3. List of Five Numerical Experiments Forced by the Different Combination of the 6-Hourly NCEP/NCAR Wind Stress, Monthly Mean Heat and Freshwater Fluxes, Climatologically Time-Mean Freshwater Discharge From 12 Major Rivers, a Parameterized Vortex Associated With Mitch, Storm-Induced Freshwater Discharge From Five Major Rivers in Honduras and Guatemala, and Storm-Induced Precipitation During Mitch[a]

Name of Run	External Forcing
Exp-Control	NCEP + MF + avgRiver + Vortex + Flood + Precipitation
Exp-Norm	NCEP + MF + avgRiver
Exp-bigRunoff	NCEP + MF + avgRiver + Vortex + Flood + Precipitation
Exp-avgRunoff	NCEP + MF + avgRiver + Vortex + Precipitation
Exp-noRain	NCEP + MF + avgRiver + Vortex + Flood

[a]Notation: 6-hourly NCEP/NCAR wind stress, NECP; monthly mean heat and freshwater fluxes, MF; climatologically time-mean freshwater discharge from 12 major rivers, avgRiver; parameterized vortex associated with Mitch, Vortex; storm-induced freshwater discharge from five major rivers in Honduras and Guatemala, Flood; storm-induced precipitation, Precipitation.

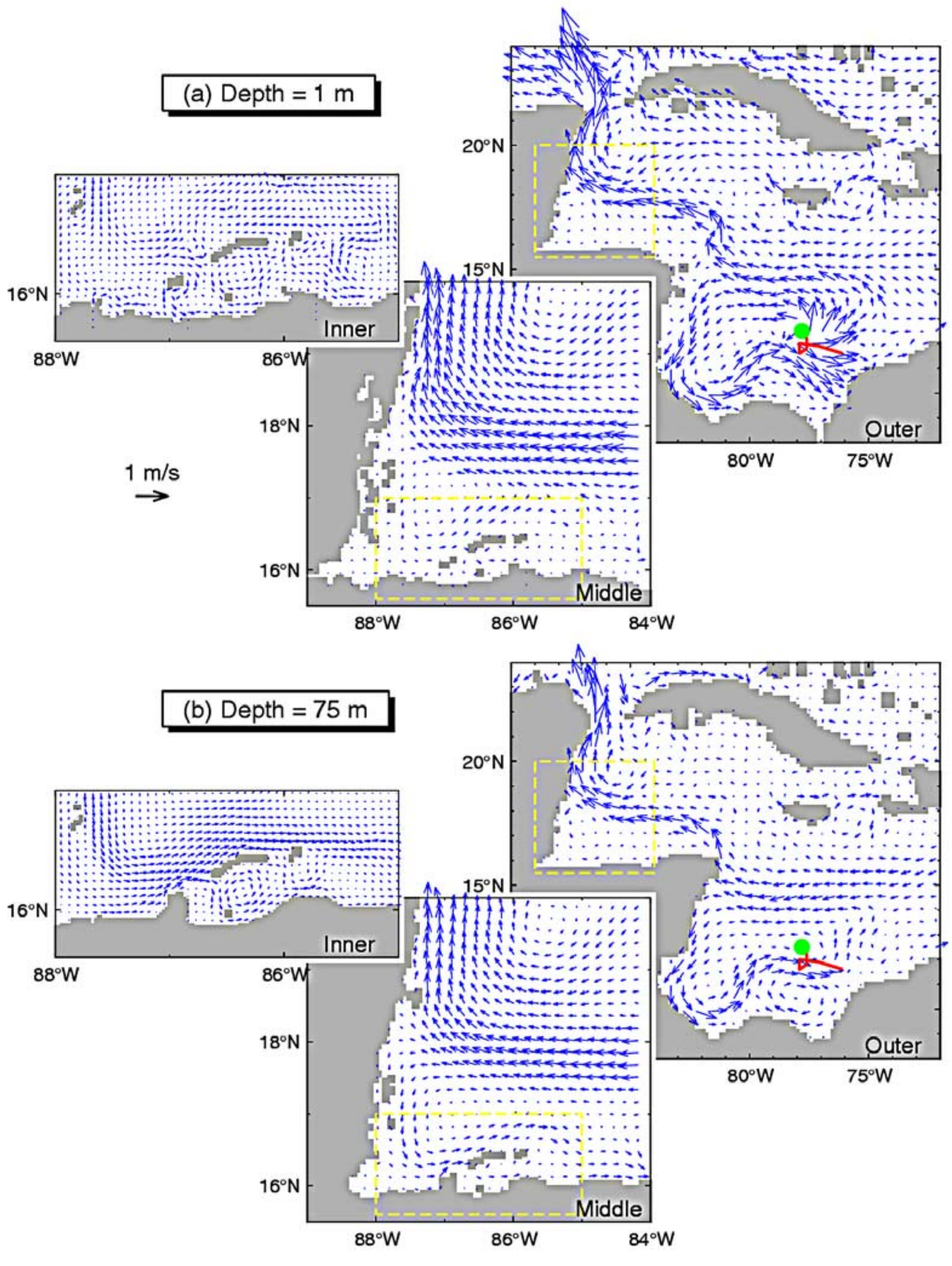

Figure 9. Simulated currents in the control run of the three-submodel system at: (a) 1 m and (b) 75 m at day 295.5 (1200 UTC 23 October) of 1998 when Hurricane Mitch intensified quickly from a tropical depression to a hurricane with sustained wind speeds of about 95 km h^{-1} in the southern Caribbean Sea. The red line represents the storm track, and the solid green circle represents the location of the storm center at this time. Velocity vectors are plotted at every third model grid point.

simulated by the middle and outer submodels are similar to the normal (no storm) conditions, which are characterized by a relatively broad, westward flow associated with the Caribbean Current in the northern and central Colombian Basin. This flow bifurcates near the Nicaragua Rise, with the main branch turning northwestward onto the southern MBRS; and a weak branch veering southwestward to feed the cyclonic Panama-Colombia Gyre over the southwestern Colombian Basin [*Mooers and Maul*, 1998; *Sheng and Tang*, 2003, 2004]. As yet unaffected by Mitch, the typical Caribbean Current flows northwestward from the Nicaragua Rise to the continental shelf off southeastern Mexico, and then turns northeastward along the east coast of the Yucatan Peninsula [*Ezer et al.*, 2005; *Tang et al.*, 2006].

[35] The simulated subsurface (75 m) circulation on 22 and 23 October (days 294 and 295) is not significantly

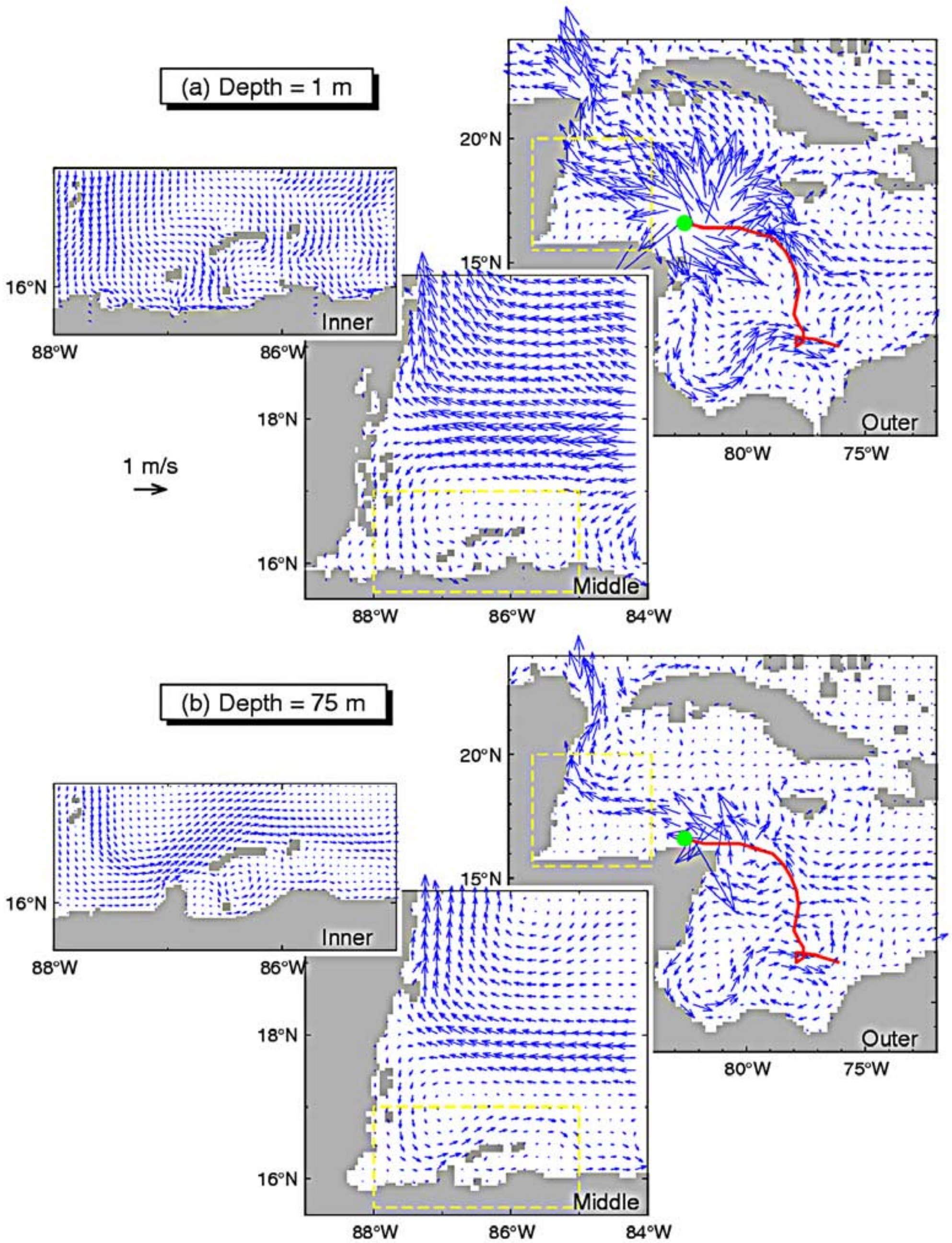

Figure 10. Simulated currents in the control run of the three-submodel system at: (a) 1 m and (b) 75 m at day 298.5 (1200 UTC 26 October) of 1998 when Mitch strengthened significantly with a maximum sustained wind speed of about 290 km h^{-1} over the Nicaragua Rise of the western Caribbean Sea. The red line represents the storm track, and the solid green circle represents the location of the storm center at this time. Velocity vectors are plotted at every third model grid point.

affected by Mitch (Figure 9b) because little storm-induced energy has penetrated into deep layers. The deeper flow at this time is westward over the northern Colombian Basin, with a large cyclonic recirculation over the southwestern Basin and several small-scale gyres near the coastal waters off Panama and Colombia (Figure 9b). Part of the westward flow runs into the central Cayman Basin through the outer flank of the Nicaragua Rise, which turns gradually into the central MBRS, and then veers anticyclonically to form an intense, narrow coastal jet running northward along the east coast of the Yucatan Peninsula.

[36] At day 298.5 (1200 UTC October 26) the vortex reaches the northern flank of the Nicaragua Rise, and the simulated near-surface currents in the WCS are significantly affected by the vortex (Figure 10a). At this time the model results are characterized as intense, divergent currents under the storm over the Cayman Basin, and strong near-inertial currents in the wake of the storm over the northern Colom-

bian Basin. These results are consistent with previous studies of storm-induced circulations [*Chang and Anthes*, 1978; *Price*, 1981; *Greatbatch*, 1983; *Sheng et al.*, 2006]. The vortex also induces a broadly westward flow exceeding 0.5 m s^{-1} velocity in the central region of the MBRS. Most of this flow turns northward along the east coast of Mexico, and the rest veers cyclonically to form a gyre in the GOH. Strong, southward coastal currents are predicted on the inner Belize shelf in the middle and inner submodels, with near-surface currents converging on the Honduran coast south of the Bay Islands (Figure 10a).

[37] The maximum subsurface currents at 75 m depth on day 298.5 produced by the outer model are ~3 m s^{-1} over the northwestern flank of the Nicaragua Rise (Figure 10b), showing the impact of the vortex on the circulation in the northwestern Colombian Basin and southern Cayman Basin. The subsurface circulations in the central and southern MBRS on day 298.5 and day 295.5 are very similar, indicating that the storm-generated energy has not penetrated very deep in the region.

[38] As the vortex approaches the north coast of Honduras on October 29, the nested-grid outer model produces intense, divergent near-surface currents of ~4 m s^{-1} between the Bay Islands and the Honduran coast, strong northwestward currents in the western Yucatan Basin, and intense northward flow through the Yucatan Strait (Figure 11a). Our results are consistent with previous findings of *Oey et al.* [2006]. They demonstrated that the northward transport across the Yucatan Strait can be significantly modified by a Caribbean hurricane. The middle and inner models generate stronger near-surface currents in the southern MBRS than does the outer model (Figure 11a), which is expected. Westward and northwestward currents of ~2 m s^{-1} occur in the central MBRS and a strong, southwestward jet is apparent over the Belize shelf. The model results also demonstrate the significant influence of the vortex on circulations at 75 m depth on day 301.0 (Figure 11b). Energy imparted by the vortex disturbs the subsurface circulation in the southern MBRS and off the Yucatan coast by this time. The middle and inner submodels generate strong, southward currents at depth on the Belize shelf, and complicated subsurface circulation features in the coastal waters around the Bay Islands.

[39] On day 304.5 (1200 UTC 1 November) about 3 days after landfall, the near-surface and subsurface circulations produced by the outer model still have strong, near-inertial currents along the storm track, particularly adjacent to the right side (Figure 12a). Broad, approximately northwestward currents are simulated for the central MBRS, with strong, eastward coastal currents north of Honduras and around the Bay Islands, and exceptional northerly flow velocities through the western Yucatan Strait.

[40] An important characteristic of storm-induced circulations is the near-inertial oscillations excited by the disturbance, which are most energetic to the right of the storm track [*Greatbatch*, 1983; *Sheng et al.*, 2006]. The effect is demonstrated here using the outer model by comparing the time-depth distributions of eastward components of the velocity in Exp-Control and Exp-Norm model runs from day 294 to 321 (Figure 13) at sites A, B and C over the deep water region between the Honduras Rise and Jamaica (Figure 1). These three sites are on the right side of the storm track and ~180 km away from the storm center. Before day 297.0 these model results do not differ between the control and normal runs. After day 297.5 at site A (or after day 298.0/299.0 at site B/C), the eastward components of the modeled velocity differences have dominant oscillations in the top 100 m with periods of about 45.0, 42.2, 39.7 hours respectively at sites A, B and C (Figure 14). These surface-intensified oscillations last for more than 20 days with amplitudes decreasing through time. The periods of the dominant oscillations are comparable to, and slightly longer than the periods of inertial oscillations defined as $2\pi/f$ (where f is the Coriolis parameter) at these three sites, namely 40.4 h, 38.4 h and 27.6 h, respectively. The fact that the dominant oscillation periods are slightly longer than the inertial oscillation periods at these sites can be explained by the interaction of the near-inertial oscillations with the background currents [*Zhai et al.*, 2005].

[41] The currents, temperatures, and salinities simulated at a single grid cell in the eleventh (25 m) *z*-level of the middle model (Figure 15) during the storm are consistent in pattern and trend with the 18-day time series collected at 27 m depth at Gladden Spit (Figure 3). Intense, variable currents, depressed temperatures in the wake of the storm, and decreased salinity associated with fresh water inputs from the coast are seen in both the modeled and the measured data. The field observations show discernable variation at tidal frequencies that was not captured by the model, which does not include tidal forcing. Reasons for the apparent discrepancies reflect mismatches between the spatial and integration timescales, inaccuracies of the model external forcing (surface winds and heat/freshwater fluxes), and the crude representation of bottom topography around the observation site, which lies outside the fine-resolution (inner model) domain. The cell dimension of the middle model (6 km × 6 km) does not resolve this structure, and the nested-grid system does not include tidal forcing. Direct comparisons at this scale are therefore of dubious value. Furthermore, the monthly mean climatological sea-surface heat is used to drive the model's surface density field, which helps explain the differences in the mean values of observed and simulated temperature.

4.2. Simulated Sea Surface Temperature

[42] Another important characteristic of the upper ocean response to a hurricane is the generation of a cool wake behind and to the right of the storm track [*Chang and Anthes*, 1978; *Price*, 1981; *Greatbatch*, 1983]. The degree of SST cooling appears to be inversely related to the hurricane translation speed, with greater cooling by a slower moving storm. Simulated near-surface temperatures predicted by the outer submodel in the control run (Figure 16) was spatially uniform at ~28°C over most of the WCS on 23 October (day 295.5) as predicted under normal forcing [*Sheng and Tang*, 2003]. There is a pool of cool surface water, however, behind the vortex over the southern Colombian Basin (Figure 16a). This feature is attributed to the intense vertical mixing associated with the storm, the translational speed of which is about 8 km h^{-1} on average from noon on 22 October to the evening of 24 October. Two other cool pools located over the Campeche Bank off the northern Yucatan Peninsula and in the

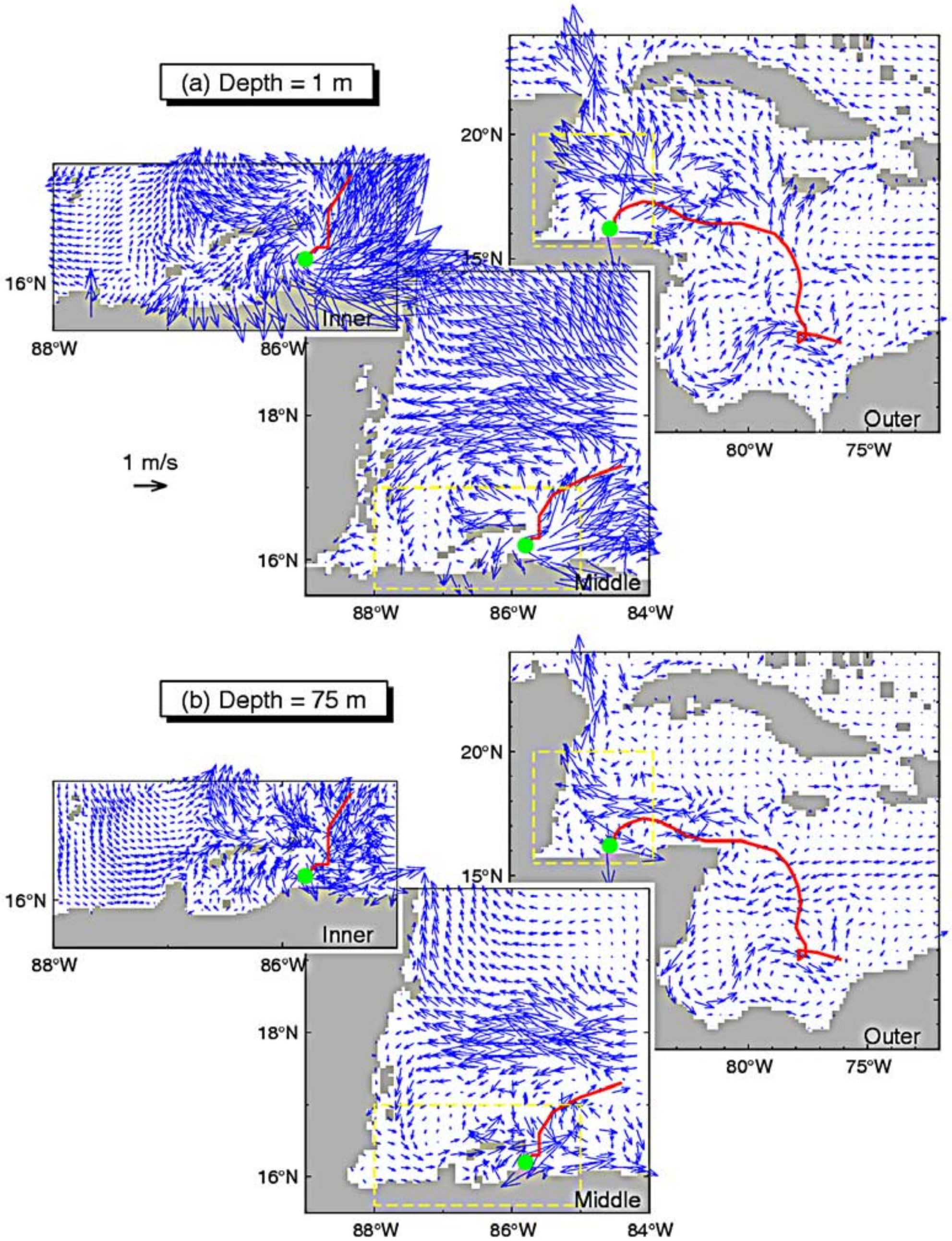

Figure 11. Simulated currents in the control run of the three-submodel system at: (a) 1 m and (b) 75 m at day 301.0 (0000 UTC 29 October), just before Mitch made landfall on the northern Honduras coast with a sustained wind speed of 205 km h^{-1}. The red line represents the storm track, and the solid green circle represents the location of the storm center at this time. Velocity vectors are plotted at every third model grid point.

coastal waters off northern Colombia are associated with the intense coastal upwelling [*Sheng and Tang*, 2003].

[43] As the vortex moves northward and then northwestward over the next three days at a mean speed of 15 km h^{-1}, its intensity increases from category 3 to category 4. A narrow strip of near-surface cooling in Colombian Basin and the northern flank of Nicaragua Rise is simulated by the outer model on 26 October (Figure 16b). Besides being more intense to the right of the storm track, the simulated wake shows significant spatial variability along the track due to variations in the translational speed of the storm. The speed of the storm slows to less than 5 km h^{-1} from 28 to 30 October, which results in a new area of simulated SST cooling to ∼20°C in the southern MBRS (Figure 16c). More than 3 days after the vortex makes landfall (1 November, day 304.5), the model results still show significant SST cooling effects of a few degrees in the WCS and more in the southern MBRS (Figure 16d).

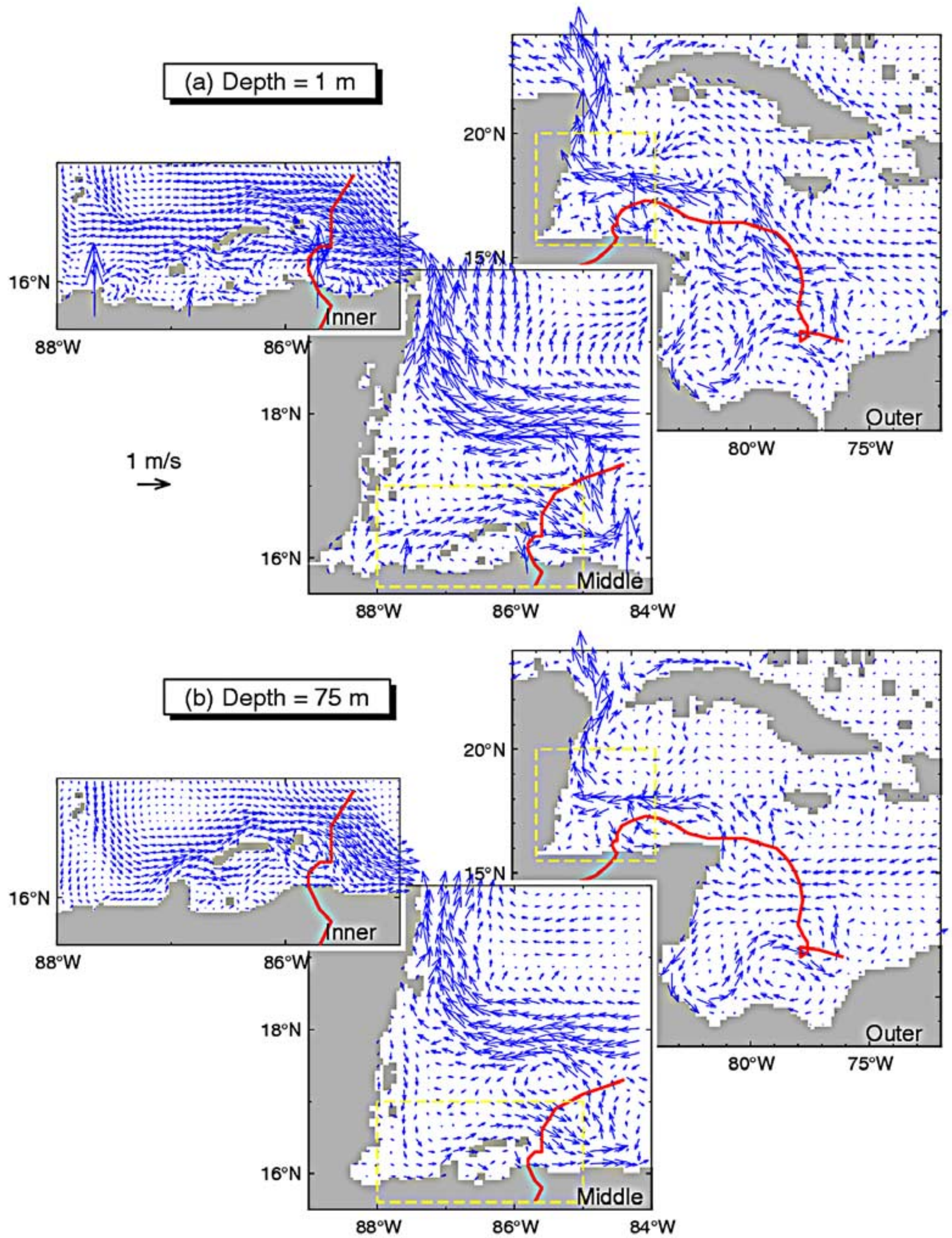

Figure 12. Simulated currents in the control run of the three-submodel system at: (a) 1 m and (b) 75 m at day 304.5 (1200 UTC 1 November) of 1998 when Mitch moved through southwestern Nicaragua and weakened to a tropical depression. The red line represents the storm track. Velocity vectors are plotted at every third model grid point.

[44] Differences in simulated near-surface temperature and currents between the Exp-Control and Exp-Norm model runs are calculated to quantify the thermal impact of Hurricane Mitch (Figure 17). As the storm advanced from day 295.5 to day 301.0, the strength of divergent currents simulated under the storm intensified by a factor of at least 5, and the amount of SST cooling in the storm's wake and the width of that cooled wake increased by as much as 36%. The size of the cool water pool, the magnitude of its anticyclonic displacement and the frequency of the near-inertial oscillations all vary within a factor of 3 as a function of variation in the translational speed of the hurricane (Figures 17a–17c). Part of the hydrodynamic energy excited by the storm propagates southward, and following the passage of the storm overland out of the model domain the simulated near-inertial currents and near-surface cooling have largely dissipated and spread to other regions of the WCS (Figure 17d).

[45] These results are consistent with other published hurricane simulations and observations. Vertical mixing

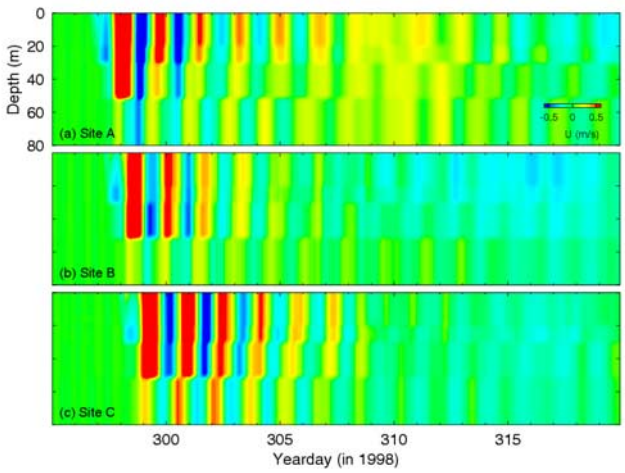

Figure 13. Time-depth distributions of eastward components of velocity differences between Exp-Control (control run) and Exp-Norm at sites A, B, and C produced by the outer model of the nested-grid system. The positions of the three sites are marked in Figure 1.

plays a dominant role in the storm-induced SST changes and the rightward bias behind a storm, while (horizontal and vertical) advection terms play a very minor role [*Sheng et al.*, 2006]. The rightward bias of the near-inertial currents and SST cooling behind the storm can be explained largely by the fact that a more efficient energy transfer from the storm to the ocean occurs on the right side of the storm track than that on the left side of the storm track (in the Northern Hemisphere) [*Chang and Anthes*, 1978; *Price*, 1981; *Greatbatch*, 1983]. This is because the wind stress veers anticyclonically at a fixed point on the right side of the storm track as the storm passes by, while the wind stress veers cyclonically on the left side of the storm track. The Coriolis term turns the ocean currents in the same direction as the wind stress on the right side of the storm track, leading to an efficient transfer of energy from the storm to the ocean currents. By contrast, on the left side of the storm track, the ocean currents are turned in the opposite direction to the wind stress, thereby weakening them. In addition, water parcels on the right side of the storm are accelerated by the wind-forcing for a longer time than those on the left side of the storm. The rightward bias of the intense, near-inertial currents behind the storm leads to stronger mixing and entrainment on the right side of the storm track, which, in turn, is mainly responsible for the rightward bias of SST cooling.

4.3. Simulated Near-Surface Salinity and River Plumes

[46] Simulations of buoyancy-driven flows of storm water inputs at the coastal boundary of the model system are evaluated by comparing the simulated sea surface salinity (SSS) in the control run with SSS derived from the SeaWiFS ocean color data. SeaWiFS images show a river plume extending from the northeastern Honduran coast to the deep ocean during Hurricane Mitch (Figure 18a), with a derived SSS of <35.5 psu. The feature is captured well by the middle model (Figure 18). Indeed, the SSS measured 2 km east of Gladden Spit on day 338 show that a low-salinity layer (~34 psu in the upper 23 m, Figure 4a) persisted for a month after the passage of Hurricane Mitch.

[47] The nested-grid middle model approximately simulates two low SSS plumes off the northern coast of Honduras on November 1 (day 304.5), as in the SeaWiFS images (Figures 18a and 18b). The western plume from the Ulua, Motagua, Cangrejal, and Bonito rivers spreads

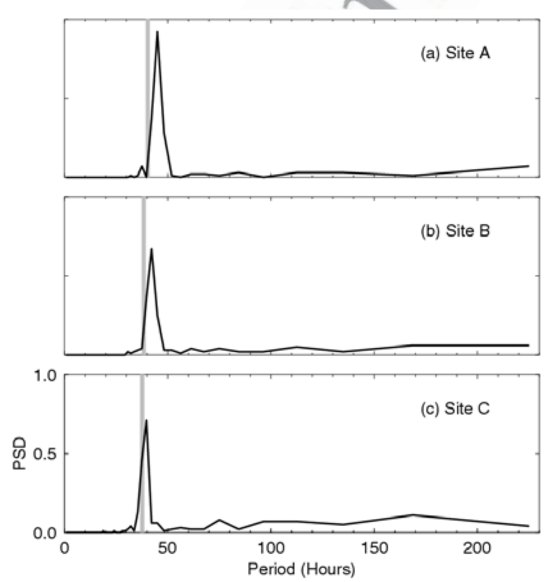

Figure 14. Power density functions at sites A, B, and C calculated from eastward components of the near-surface velocity differences produced by the outer model of the nested-grid system. The shaded line represents the period of inertial oscillation at each site. The positions of the three sites are marked in Figure 1.

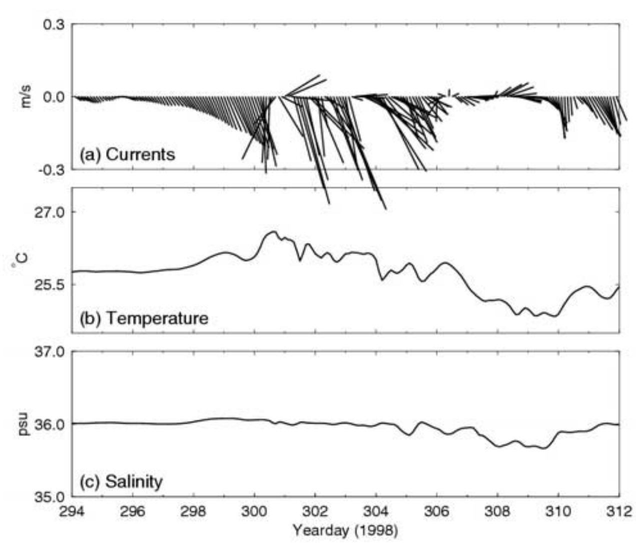

Figure 15. Simulated currents, temperature, and salinity in the 15-m-deep cell (z-level 8) at 87.95°W and 16.5°N, off Gladden Spit at the southern end of the Belize Barrier Reef (see Figure 1) over an 18-day time series (22 October to 8 November) spanning the passage of Hurricane Mitch through the area.

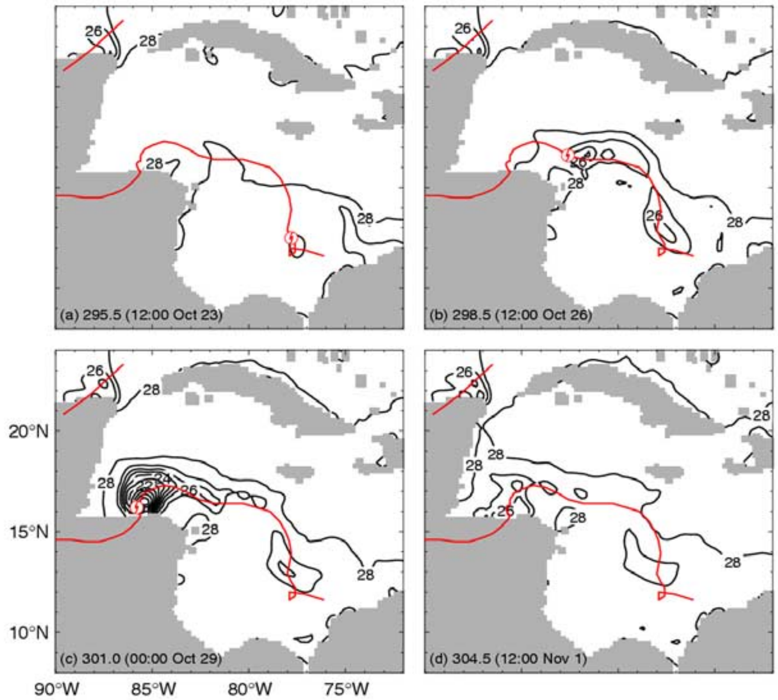

Figure 16. Simulated sea surface temperature (SST) associated with Hurricane Mitch at different times produced by the outer model of the nested system. Contour intervals are 1°C. The red line represents the storm track and the symbol shows the position of the storm center.

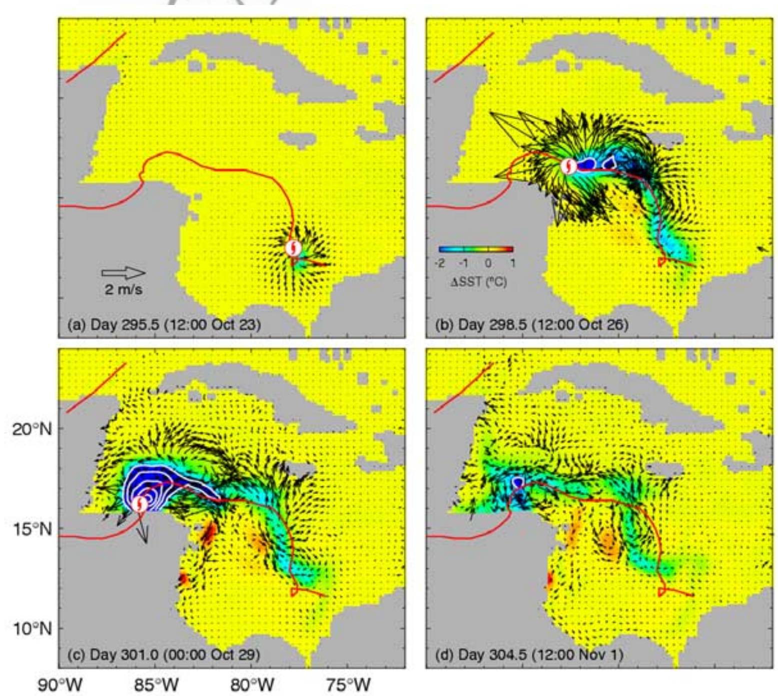

Figure 17. Model-calculated changes in sea surface temperature (ΔSST) and currents associated with Hurricane Mitch at different times produced by the outer model of the nested system. Contour intervals are 2°C. The red line represents the storm track, and the storm symbol represents the location of the storm center. Velocity vectors are plotted at every second grid point.

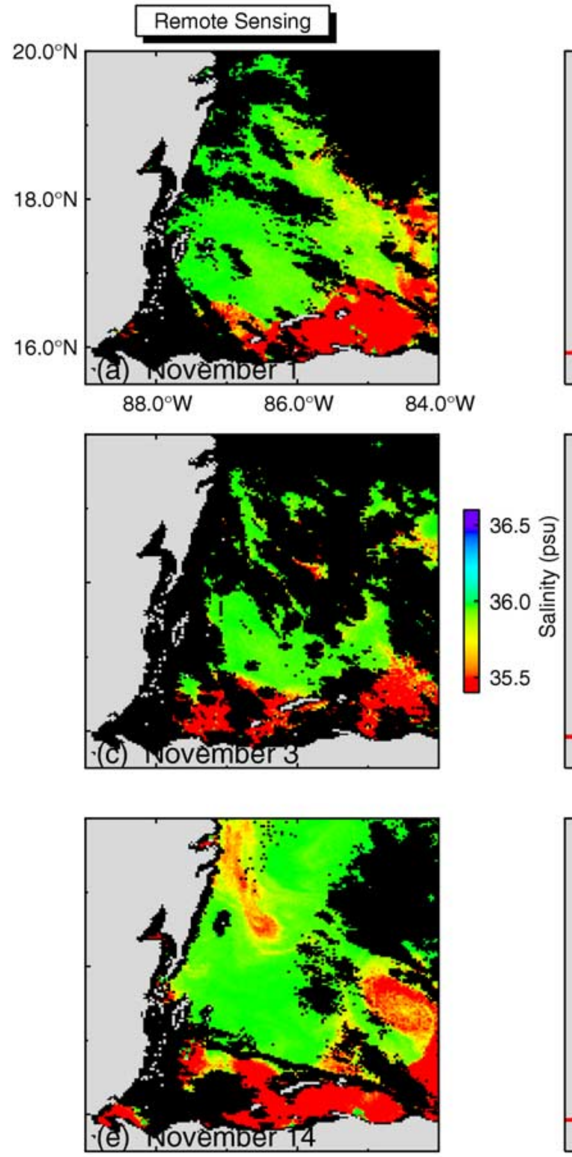

Figure 18. Comparison of spatial patterns of river plumes characterized by the sea surface salinity field between (a, c, e) the SeaWiFS data and (b, d, f) the middle model results on three dates during Hurricane Mitch. Clouds are masked as black color in Figures 18a, 18c, and 18e. Model velocity vectors are plotted at every third grid point.

northeastward, reaching the Bay Islands within a day. The eastern plume from the Aguan and Patuca rivers on the northeastern Honduran coast also spreads rapidly to interact with the Caribbean Current in deep water northeast of the Bay Islands. A backward breaking wave in the upstream direction along the outer edge of this plume (Figure 18b) is a typical feature of baroclinic waves on a density front [*Sheng*, 2001]. Both the western and eastern plumes continue to expand and deform in simulations over the next few days, such that they merge in a pool of low-salinity waters along the northern coast of Honduras by November 14 (day 317.5), well after the hurricane's passage (Figures 18c–18f). The leading portion of the eastern plume has separated from the main body of the plume by this time, entrained in a cyclonic gyre north of the Bay Islands (Figure 18f). Normal salinity (>36) was apparently restored in the GoH by 7 May (Figure 4b), approximately 6 months after the storm.

[48] The nested-grid modeling system is insensitive to the difference in the flood processes specified in Exp-Control (control run) and Exp-bigRunoff before day 305.0, but large differences occur between the two runs in the model-calculated SSS and the estuarine plumes by day 327.5 (Figures 19a and 19b). The eastern plume produced by the outer model in Exp-bigRunoff is unrealistically large in comparison with the SeaWiFS imagery [*Andréfouët et al.*, 2002], while the river plumes produced by the Exp-avgRunoff model run are unrealistically small (Figures 19a and 19c). The control run seems to be the best in simulating salinity patterns within the plumes, with relatively lower SSS in the northeastern part of the middle model domain

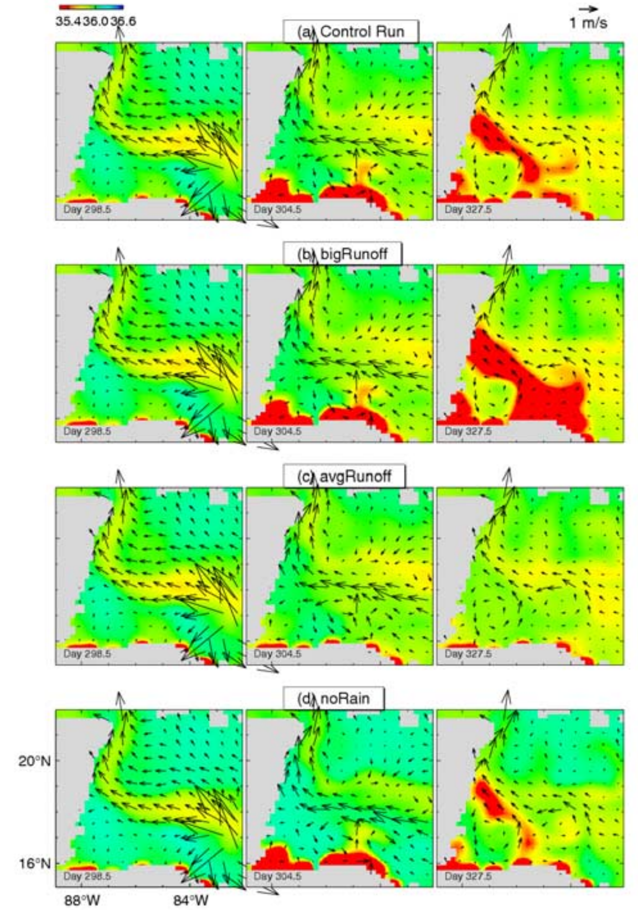

Figure 19. Near-surface salinity fields produced by the outer model of the nested-grid system in four experimental runs (see Table 3): (a) Exp-Control, (b) Exp-bigRunoff, (c) Exp-avgRunoff, and (d) Exp-noRain. Model velocity vectors are plotted at every third grid point.

and higher SSS in the central MBRS and Belize shelf, in agreement with SeaWiFS data (Figure 18). This low-salinity surface water is generated by storm-induced precipitation, as it is absent in the Exp-noRain model run (Figures 19a and 19d), demonstrating the importance of precipitation on coastal density structure and circulation during the hurricane.

5. Summary and Discussion

[49] A triply nested-grid ocean circulation modeling system, evaluated with SeaWiFS imagery and in situ oceanographic observations, was used to study the dynamic response of the upper ocean in the Mesoamerican Barrier Reef System (MBRS) to the passage of Hurricane Mitch through the region in late October 1998. The model wind-forcing was approximated by a parameterized vortex inserted into the coarse-resolution NCEP/NCAR wind fields. The nested-grid system simulated reasonably well the highly localized, intense, divergent currents forced by the local wind under the storm, the intense near-inertial currents and cooling of sea surface temperature (SST) behind the storm track, and the bias of the near-inertial currents and SST cooling to the right of the storm track. The rightward bias of the near-inertial currents behind the storm is mainly due to the fact that there is a more efficient energy transfer from the storm to the ocean on the right side of the storm track than that on the left side of the storm track [*Chang and Anthes*, 1978; *Greatbatch*, 1983]. The rightward bias of the near-inertial currents behind the storm leads to stronger entrainment and mixing on the right side of the storm track, which is the main reason for the rightward bias of SST cooling [*Price*, 1981; *Sheng et al.*, 2006].

[50] Storm-induced near-inertial currents are relatively strong and widespread over much of the northwestern Caribbean Sea, and in the vicinity of the storm track over the central Colombian Basin. Part of the near-inertial energy excited over the northern flank of the Nicaragua Rise propagates southward along the east coast of Honduras and reaches the southwestern Colombian Basin by the time the hurricane made landfall. Four days later, however, the SST cooling and near-inertial currents have largely dissipated and spread to other regions of the western Caribbean Sea (WCS). The nested-grid system also produced a large area of SST cooling in the southern MBRS, with a maximum thermal loss of about 10°C over the coastal region around the Bay Islands, and weaker SST cooling over the northern flank of the Nicaragua Rise and central Colombian Basin.

[51] Because of heavy precipitation associated with Hurricane Mitch and the extensive coastal boundary in the study region, it was essential to include buoyancy forcing associated with storm-induced river discharge and precipitation over the WCS during and after the storm in the model simulations. We made use of remotely sensed imagery, meteorological data and watershed model outputs to approximate the buoyancy forcing associated with storm-induced precipitation in the open ocean of the WCS and flood river runoff at the coastal margins. Sea surface salinity (SSS) was derived empirically by assuming an inverse relationship between SSS and colored dissolved organic matter detected by the SeaWiFS satellite. Parameterized flood processes during Mitch were constructed for five major rivers in Honduras and Guatemala from published observations and models [*Smith et al.*, 2002; *Thattai et al.*, 2003]. The nested-grid system generated patterns of river plume evolutions that were comparable with the SeaWiFS observations in both space and time. Domain-scale patterns of advection from coastal areas to the northernmost regions of the MBRS within days were produced as a result of the massive storm disturbance event. The entire northern shelf of Honduras was inundated by low-salinity estuarine waters, and the buoyant estuarine plumes were entrained in post-storm circulations that extended hundreds of kilometers to the north and northwest. The fine structures of the plumes as well as the absolute salinity values within the plumes produced by the model, however, depend strongly on the accuracy of the flood processes and upper ocean circulations in the region that deserve further studies.

[52] Validation of model results is problematic in the MBRS because of the sparse and unsystematic observations in the region. In situ observation during hurricane conditions is difficult to obtain without arrays of permanent moorings in place in advance. The lack of multiple locations of in situ observations was compensated for in part by using

synoptic SeaWiFS observations before and after Mitch to evaluate the model simulations using qualitative comparisons of the spatial extent of river plumes. Comparison of simulated currents, temperature and salinity in a single cell of the middle model with the only available empirical measurements of ocean conditions in the MBRS during the storm shows that while the magnitudes and temporal pattern of change in the simulated current velocities and temperatures associated with the storm passage are approximately consistent with the 18-day time series collected at 27 m near Gladden Spit, the simulated salinity does not capture the variability or trend apparent in the observed time series.

[53] The spatial and temporal resolution and reasonable representation of model forcing of the nested-grid model system permit reasonable simulations of the proximal and distal effects of Hurricane Mitch on patterns of physical connectivity within an ecologically defined coral reef province. These are determined through comparisons with the climatological mean situation elucidated using the same model system as *Tang et al.* [2006]. The major impacts of the storm event were to strongly mix and rapidly diverge the waters of the upper ocean adjacent to the storm track, and to greatly accelerate and increase the flow of water from the southeastern portion of the MBRS region onto the atolls and barrier reef structures to the northwest.

[54] The magnitude of these impacts relative to the climatological mean scenario for the October–December period was large and persistent. Divergent near-surface velocities were 7 to 13 times higher within a 250 km radius of the storm center for a 5 day period. Subsurface flows at 75 m depth were also about 5 times faster and less uniformly directed within the storm radius. The SST over areas as large as 60,000 km^2 in the wake of the storm track was 7% to 36% colder for periods as long as 15 days. The intense vertical mixing and vertical advection (upwelling) associated with this SST cooling draw waters from as deep as 100 m. The northeastward flows associated with the buoyant plumes flooded the northern Honduran shelf to a distance of 70 km offshore for 2 weeks after the storm passage, and then extended northwest more than 230 km from the coast to the deep ocean atolls and into the Belize barrier reef matrix at rates approximately 3 times faster than the climatological mean velocities. Signatures of hydrographic features and storm-induced flows associated with the hurricane were still evident more than 30 days after the passage of the storm. In addition to the significant insertions of near-inertial energy and modifications of the upper-ocean density structure to the southern MBRS, Hurricane Mitch produced significant deviations from the climatological mean circulation in the region: an intense easterly reversal of flow across the Honduran shelf as the storm approached; a major enhancement of the northerly flow off the Honduran shelf both during the storm and afterward in reduced salinity plumes shifting toward the west; and a complete disruption of the gyre in the GOH.

[55] Translating the simulated hydrodynamics in the MBRS into predictions of impacts of Hurricane Mitch on ecological connectivity in the region poses challenges beyond the scope of this paper. The timescale of the storm event (5–15 days) is shorter, but of the same order as the pelagic larval duration of many Caribbean corals and reef fish [*Szmant and Meadows*, 2006; *Leis and McCormick*, 2002]. Reproductive propagules (spores, eggs and early stage larvae) may be modeled as conservative with respect to the water mass for only the first 5–10 days following release, after which they are progressively more capable of directed vertical and horizontal movement. Water velocities in excess of 1 cm s^{-1}, however, will advect even the most competent swimmers [*Fisher*, 2005].

[56] Future work on numerical studies of the three-dimensional circulation and hydrodynamic connectivity in the MBRS includes better representations of the shallow reef topography and rugosity using high-resolution remote sensing data [*Andréfouët et al.*, 2003], and more accurate specification of the coastal salinity waters with in situ measurements along the Honduras, Guatemala and Belize coasts. Simulations of additional scenarios that characterize coastal circulation patterns visualized in remotely sensed imagery are also required to calibrate model results under both short-lived, 'catastrophic' and long-term mean, 'normal' conditions. Sensitivity analyses, in combination with better representation of reef morphometrics relative to hydrodynamic forcing [e.g., *Naseer and Hatcher*, 2001, 2004] will improve the skill of numerical models and enhance the quantitative matching of model result to synoptic image.

[57] **Acknowledgments.** We wish to thank Liqun Tang, Richard Greatbatch, Xiaoming Zhai, Chris Fogarty, Tel Ezer, and two anonymous reviewers for their very useful suggestions. This project is supported by NASA Interdisciplinary Program grant NNG04GO90G. Field measurements along the Mesoamerican Reef were supported by UNESCO, United Nations Development Programme (UNDP), The Nature Conservancy (TNC), the Mesoamerican Barrier Reef System (MBRS) Project of the World Bank, and the Mellon Foundation.

References

Andréfouët, S., P. J. Mumby, M. McField, C. Hu, and F. E. Muller-Karger (2002), Revisiting coral reef connectivity, *Coral Reefs*, *21*, 43–48.

Andréfouët, S., et al. (2003), Multi-sites evaluation of IKONOS data for classification of tropical coral reef environments, *Remote Sens. Environ.*, *88*, 128–143.

Barnier, B., L. Siefridt, and P. Marchesiello (1995), Thermal forcing for a global ocean circulation model using a three-year climatology for ECMWF analyses, *J. Mar. Syst.*, *6*, 363–380.

Burke, L., and Z. Zugg (2006), Hydrologic modeling of watersheds discharging adjacent to the Mesoamerican reef, report, 35 pp., World Resour. Inst., Washington, D. C.

Chang, S. W., and R. A. Anthes (1978), Numerical simulations of the ocean's nonlinear baroclinic response to translating hurricanes, *J. Phys. Oceanogr.*, *8*, 468–480.

Cornillon, P., L. Stramma, and J. F. Price (1987), Satellite measurement of sea surface cooling during Hurricane Gloria, *Nature*, *326*, 373–375.

Cowen, R. K., C. B. Paris, and A. Srinivasan (2006), Scaling of connectivity in marine populations, *Science*, *311*, 522–527.

Craig, A. K. (1966), *Geography of Fishing in British Honduras and Adjacent Coastal Waters*, 143 pp., La. State Univ. Press, Baton Rouge.

da Silva, A. M., C. C. Young, and S. Levitus (1994), *Atlas of Surface Marine Data 1994*, vol. 3, *Anomalies of Heat and Momentum Fluxes*, *NOAA Atlas NESDIS*, vol. 8, 413 pp., NOAA, Silver Spring, Md.

Dietrich, D. E. (1997), Application of a modified Arakawa 'a' grid ocean model having reduced numerical dispersion to the Gulf of Mexico circulation, *Dyn. Atmos. Oceans*, *27*, 201–217.

D'Sa, E. J., C. Hu, F. E. Muller-Karger, and K. L. Carder (2002), Estimation of colored dissolved organic matter and salinity fields in case 2 waters using SeaWiFS: Examples from Florida Bay and Florida Shelf, *Proc. Indian Acad. Sci. Earth Planet Sci.*, *111*, 197–207.

Ezer, T., L.-Y. Oey, and H.-C. Lee (2003), The variability of currents in the Yucatan Channel: Analysis of results from a numerical model, *J. Geophys. Res.*, *108*(C1), 3012, doi:10.1029/2002JC001509.

Ezer, T., D. V. Thattai, B. Kjerfve, and W. D. Heyman (2005), On the variability of the flow along the Meso-American Barrier Reef System:

A numerical model study of the influence of the Caribbean current and eddies, *Ocean Dyn.*, *55*, 458–475, doi:10.1007/s10236-005-0033-2.

Fedorov, K. N., A. A. Varfolomeev, A. I. Ginzburg, A. G. Zatsepin, A. Y. Krasnopevtsev, A. G. Ostrovsky, and V. E. Skylarov (1979), Thermal reaction of the ocean on the passage of Hurricane Ella, *Okeanologiya*, *19*, 992–1001.

Ferrari, G. M., and M. D. Dowell (1998), CDOM absorption characteristics with relation to fluorescence and salinity in coastal areas of the southern Baltic Sea, *Estuarine Coastal Shelf Sci.*, *47*, 91–105.

Fisher, R. (2005), Swimming speeds of larval coral reef fishes: Impacts on self-recruitment and dispersal, *Mar. Ecol. Prog. Ser.*, *285*, 223–232.

Geshelin, Y., J. Sheng, and R. J. Greatbatch (1999), Monthly mean climatologies of temperature and salinity in the western North Atlantic, report, *Can. Tech. Rep. Hydrogr. Ocean. Sci*. *153*, 62 pp., Fish. and Oceans, Ottawa, Ont., Canada.

Greatbatch, R. J. (1983), On the response of the ocean to a moving storm: The nonlinear dynamics, *J. Phys. Oceanogr.*, *13*, 357–367.

Guiney, J. L., and M. B. Lawrence (1999), Preliminary report: Hurricane Mitch 22 October–5 November 1998, report, 8 pp., Natl. Hurricane Cent., Miami, Fla.

Hatcher, B. G. (1997), Coral reef ecosystems: How much greater is the whole than the sum of the parts?, *Coral Reefs*, *16*, 77–91.

Hatcher, B. G., M. Coreless, R. Goodridge, and S. Scott (2004), Testing mechanisms by which marine protected areas export fish to adjacent habitats: The Soufriere Experiment in Reef Fisheries Sustainability (SERFS), *Proc. Annu. Gulf Caribb. Fish. Inst.*, *48*, 273–292.

Heyman, W. D., and B. Kjerfve (2000), The Gulf of Honduras, in *Coastal Ecosystems of Latin America*, *Ecol. Stud.*, vol. 144, edited by U. Seeliger and B. Kjerfve, pp. 17–32, Springer, Berlin.

Hu, C., F. E. Muller-Karger, D. C. Biggs, K. L. Carder, B. Nababan, D. Nadeau, and J. Vanderbloemen (2003), Comparison of ship and satellite bio-optical measurements on the continental margin of the NE Gulf of Mexico, *Int. J. Remote Sens.*, *24*, 2597–2612.

Hu, C., E. T. Montgomery, R. W. Schmitt, and F. E. Muller-Karger (2004), The dispersal of the Amazon and Orinoco River water in the tropic Atlantic and Caribbean Sea: Observation from space and S-PALACE floats, *Deep Sea Res., Part II*, *51*, 1151–1171.

Hu, C., J. R. Nelson, E. Johns, Z. Chen, R. H. Weisberg, and F. E. Muller-Karger (2005), Mississippi River water in the Florida Straits and in the Gulf Stream off Georgia in summer 2004, *Geophys. Res. Lett.*, *32*, L14604, doi:10.1029/2005GL022942.

Huffman, G. J., R. F. Adler, M. M. Morrissey, D. T. Bolvin, S. Curtis, R. Joyce, B. McGavock, and J. Susskind (2001), Global precipitation at one-degree daily resolution from multisatellite observations, *J. Hydrometeorol.*, *2*, 36–50.

Ishizaka, J. (1990), Coupling of coastal zone color scanner data to a physical-biological model of the southeastern U.S. continental shelf ecosystem, part 1: CZCS data description and Lagrangian particle tracing experiments, *J. Geophys. Res.*, *95*, 20,167–20,181.

Jordan, C. L. (1964), On the influence of tropical cyclones on the sea surface temperature, paper presented at Symposium on Tropical Meteorology, World Meteorol. Organ., Wellington.

Kalnay, E., et al. (1996), The NCEP/NCAR 40–year reanalysis project, *Bull. Am. Meteorol. Soc.*, *77*, 437–472.

Kramer, P. A., and P. R. Kramer (2002), *Ecoregional Conservation Planning for the Mesoamerican Caribbean Reef*, 140 pp., World Wildlife Fed., Gland, Switzerland.

Large, W. G., and S. Pond (1981), Open ocean momentum flux measurements in moderate to strong winds, *J. Phys. Oceanogr.*, *11*, 324–336.

Lee, Z., K. L. Carder, and R. A. Arnone (2002), Deriving inherent optical properties from water color: A multiband quasi-analytic algorithm for optically deep waters, *Appl. Opt.*, *41*, 5755–5772.

Legrand, S., E. Deleersnijder, E. Hanert, V. Legat, and E. Wolanski (2006), High-resolution, unstructured meshes for hydrodynamic models of the Great Barrier Reef, Australia, *Estuarine Coastal Shelf Sci.*, *68*, 36–46.

Leis, J., and M. McCormick (2002), The biology, behavior, and ecology of the pelagic, larval stage of coral reef fishes, in *Coral Reef Fishes: Dynamics and Diversity in a Complex Ecosystem*, edited by P. Sale, pp. 171–200, Academic, San Diego, Calif.

Marchesiello, P., J. C. McWilliams, and A. Shchepetkin (2001), Open boundary conditions for long-term integration of regional oceanic models, *J. Ocean Model.*, *3*, 1–20.

Mastin, M. C., and T. D. Olsen (2002), Fifty-year storm-tide flood-inundation maps for Santa Rosa de Aguan, Honduras, *U.S. Geol. Surv. Water Resour. Invest. Rep.*, *02-258*.

McClain, C. R., G. C. Feldman, and S. B. Hooker (2004), An overview of the SeaWiFS project and strategies for producing a climate research quality global ocean bio-optical time series, *Deep Sea Res., Part II*, *51*, 5–42.

Mooers, C. N. K., and G. A. Maul (1998), Intra-Americas Sea circulation, coastal segment (3,W), in *The Sea*, vol. 11, pp. 183–208, John Wiley, Hoboken, N. J.

Murphy, S. J., H. E. Hurburt, and J. J. O'Brien (1999), The connectivity of eddy variability in the Caribbean Sea, the Gulf of Mexico, and the Atlantic Ocean, *J. Geophys. Res.*, *104*, 1431–1453.

Naseer, A., and B. G. Hatcher (2001), Assessing the integrated growth response of coral reefs to monsoon forcing using morphometric analysis of reefs in Maldives, paper presented at Ninth International Coral Reef Symposium, Int. Soc. for Reef Stud., Melbourne, Fla.

Naseer, A., and B. G. Hatcher (2004), Inventory of the Maldives' coral reefs using morphometrics generated from Landsat ETM+ imagery, *Coral Reefs*, *23*, 161–168.

Oey, L.-Y., and P. Chen (1992), A nested-grid ocean model: With application to the simulation of meanders and eddies in the Norwegian coastal current, *J. Geophys. Res.*, *97*, 20,063–20,086.

Oey, L.-Y., T. Ezer, and H.-C. Lee (2005), Loop current, rings and related circulation in the Gulf of Mexico: A review of numerical models and future challenges, in *Circulation in the Gulf of Mexico: Observations and Models*, *Geophys. Monograph Ser.*, vol. 161, edited by W. Sturges and A. L. Fernandez, pp. 31–56, AGU, Washington, D. C.

Oey, L.-Y., T. Ezer, D.-P. Wang, S.-J. Fan, and X.-Q. Yin (2006), Loop current warming by Hurricane Wilma, *Geophys. Res. Lett.*, *33*, L08613, doi:10.1029/2006GL025873.

Oey, L.-Y., T. Ezer, D.-P. Wang, X.-Q. Yin, and S.-J. Fan (2007), Hurricane-induced motion and interaction with ocean currents, *Cont. Shelf. Res.*, *27*, 1249–1263, doi:10.10.1016/j./csr.2007.01.008.

O'Reilly, J. E., S. Maritorena, B. G. Mitchell, D. A. Siegel, K. L. Carder, S. A. Garver, M. Kahru, and C. R. McClain (1998), Ocean color chlorophyll algorithms for SeaWiFS, *J. Geophys. Res.*, *103*, 24,937–24,953.

Palumbi, S. R. (2003), Population genetics, demographic connectivity, and the design of marine reserves, *Ecol. Appl.*, *13*, S146–S158.

Powell, M. D., P. J. Vickery, and T. A. Reinhold (2003), Reduced drag coefficient for high wind speeds in tropical cyclones, schemes, *Nature*, *422*, 279–283.

Price, J. F. (1981), Upper ocean response to a hurricane, *J. Phys. Oceanogr.*, *11*, 153–175.

Sale, P. F. (2004), Connectivity, recruitment variation, and the structure of reef fish communities, *Integr. Comp. Biol.*, *44*, 390–399.

Sheng, J. (2001), Dynamics of a buoyancy-driven coastal jet: The Gaspe Current, *J. Phys. Oceanogr.*, *31*, 3146–3163.

Sheng, J., and Y. R. Rao (2006), Circulation and thermal structure in Lake Huron and Georgian Bay: Application of a nested-grid hydrodynamic model, *Cont. Shelf Res.*, *26*, 1496–1518.

Sheng, J., and L. Tang (2003), A numerical study of circulation in the western Caribbean Sea, *J. Phys. Oceanogr.*, *31*, 3146–3163.

Sheng, J., and L. Tang (2004), A two-way nested-grid ocean-circulation model for the Mesoamerican Barrier Reef System, *Ocean Dyn.*, *54*, 232–242.

Sheng, J., and L. Wang (2004), Numerical study of tidal circulation and nonlinear dynamics in Lunenburg Bay, Nova Scotia, *J. Geophys. Res.*, *109*, C10018, doi:10.1029/2004JC002404.

Sheng, J., D. G. Wright, R. J. Greatbatch, and D. E. Dietrich (1998), CANDIE: A new version of the DieCAST ocean circulation model, *J. Atmos. Oceanic Technol.*, *15*, 1414–1432.

Sheng, J., R. J. Greatbatch, and D. G. Wright (2001), Improving the utility of ocean circulation models through adjustment of the momentum balance, *J. Geophys. Res.*, *106*, 16,711–16,728.

Sheng, J., R. J. Greatbatch, X. Zhai, and L. Tang (2005), A new two-way nesting technique based on the smoothed semi-prognostic method, *Ocean Dyn.*, *55*, 162–177, doi:10.101007/sl0236-005-0005-6.

Sheng, J., X. Zhai, and R. J. Greatbatch (2006), Numerical study of the storm-induced circulation on the Scotian Shelf during Hurricane Juan using a nested-grid ocean model, *Prog. Oceanogr.*, *70*, 233–254, doi:10.1016/j.pocean.2005.07.007.

Smagorinsky, J. (1963), General circulation experiments with the primitive equation, part I. The basic experiment, *Mon. Weather Rev.*, *21*, 99–165.

Smith, M. E., J. V. Phillips, and N. E. Spahr (2002), Hurricane Mitch: Peak discharge for selected river reaches in Honduras, *U.S. Geol. Surv. Water Resour. Invest. Rep.*, *01-4266*.

Smith, N. P. (1982), Response of Florida Atlantic Shelf Waters to Hurricane David, *J. Geophys. Res.*, *87*, 2007–2016.

Szmant, A. M., and M. G. Meadows (2006), Developmental changes in coral larval buoyancy and vertical swimming behavior: Implications for dispersal and connectivity, paper presented at Tenth International Coral Reef Symposium, Int. Soc. for Reef Stud., Melbourne, Fla.

Tang, L., J. Sheng, B. G. Hatcher, and P. F. Sale (2006), Numerical study of circulation, dispersion and hydrodynamic connectivity of surface waters on the Belize shelf, *J. Geophys. Res.*, *111*, C01003, doi:10.1029/2005JC002930.

Thattai, D., B. Kjerfve, and W. D. Heyman (2003), Hydrometeorology and variability of water discharge and sediment load in the inner Gulf of Honduras, western Caribbean, *J. Hydrometeorol.*, *4*, 985–995.

Thuburn, J. (1996), Multidimensional flux-limited advection schemes, *J. Comput. Phys.*, *123*, 74–83.

United Nations Environment Programme Chemicals (2002), Regionally based assessment of persistent toxic substances in Central America and the Caribbean, report, 133 pp., Global Environ. Facil., Chatelaine, Switzerland.

Wang, L., J. Sheng, A. E. Hay, and D. J. Schillinger (2007), Storm-induced circulation in Lunenburg Bay of Nova Scotia: Observations and numerical simulations, *J. Phys. Oceanogr.*, *37*, 873–895, doi:10.1175/JPO3031.1.

Wolanski, E. (2001), *Oceanographic Processes of Coral Reefs: Physical and biological links in the Great Barrier Reef*, 356 pp., CRC Press, Boca Raton, Fla.

Zhai, X., R. J. Greatbatch, and J. Sheng (2005), Doppler-shifted inertial oscillations on a β plane, *J. Phys. Oceanogr.*, *35*, 1480–1488.

S. Andréfouët, UR 128 Coréus, Institut de Recherche pour le Développement, BP A5, 98848, Noumea Cedex, New Caledonia.

B. G. Hatcher, Centre for Marine Ecosystem Research, Cape Breton University, Sydney, NS, Canada B1P 6L2.

W. D. Heyman and B. Kjerfve, Department of Geography, Texas A&M University, College Station, TX 77843-3187, USA.

C. Hu, F. E. Muller-Karger, and L. Wang, Institute for Marine Remote Sensing, College of Marine Science, University of South Florida, St. Petersburg, FL 33701, USA.

J. Sheng and B. Yang, Department of Oceanography, Dalhousie University, 1355 Oxford Street, Halifax, NS, Canada B3H 4J1. (jinyu.sheng@dal.ca)